land

Review

Urban Heat Island and Its Regional Impacts Using Remotely Sensed Thermal Data—A Review of Recent Developments and Methodology

Hua Shi [1,*], George Xian [2], Roger Auch [2], Kevin Gallo [3] and Qiang Zhou [1]

[1] ASRC Federal Data Solutions (AFDS), Contractor to the U.S. Geological Survey (USGS) Earth Resources Observation and Science (EROS) Center, Sioux Falls, SD 57198, USA; qzhou@contractor.usgs.gov
[2] U.S. Geological Survey (USGS) Earth Resources Observation and Science (EROS) Center, Sioux Falls, SD 57198, USA; xian@usgs.gov (G.X.); auch@usgs.gov (R.A.)
[3] Center for Satellite Applications and Research, National Oceanic and Atmospheric Administration (NOAA)/NESDIS, College Park, MD 20740, USA; kevin.p.gallo@noaa.gov
* Correspondence: hshi@contractor.usgs.gov; Tel.: +1-605-594-6050

Abstract: Many novel research algorithms have been developed to analyze urban heat island (UHI) and UHI regional impacts (UHIRIP) with remotely sensed thermal data tables. We present a comprehensive review of some important aspects of UHI and UHIRIP studies that use remotely sensed thermal data, including concepts, datasets, methodologies, and applications. We focus on reviewing progress on multi-sensor image selection, preprocessing, computing, gap filling, image fusion, deep learning, and developing new metrics. This literature review shows that new satellite sensors and valuable methods have been developed for calculating land surface temperature (LST) and UHI intensity, and for assessing UHIRIP. Additionally, some of the limitations of using remotely sensed data to analyze the LST, UHI, and UHI intensity are discussed. Finally, we review a variety of applications in UHI and UHIRIP analyses. The assimilation of time-series remotely sensed data with the application of data fusion, gap filling models, and deep learning using the Google Cloud platform and Google Earth Engine platform also has the potential to improve the estimation accuracy of change patterns of UHI and UHIRIP over long time periods.

Keywords: urban heat island; UHI regional impacts; non-urban areas; remote sensing; thermal band; UHI intensity

Citation: Shi, H.; Xian, G.; Auch, R.; Gallo, K.; Zhou, Q. Urban Heat Island and Its Regional Impacts Using Remotely Sensed Thermal Data—A Review of Recent Developments and Methodology. *Land* **2021**, *10*, 867. https://doi.org/10.3390/land10080867

Academic Editors: Sara Venafra, Carmine Serio and Guido Masiello

Received: 17 July 2021
Accepted: 11 August 2021
Published: 18 August 2021

1. Introduction

Urbanization is known to have substantial impacts on landscapes and ecosystems [1–4], and urban inhabitants are expected to reach 70% of the world population by 2050 [5]. Moreover, the nature of urban development has been changing from a single city model to a group of cities (urban agglomeration) worldwide. Urban heat island (UHI), urbanization, and climate change are increasingly interconnected, resulting in several environmental consequences (such as heat stress, biodiversity loss, fire risk, warming water due to run off, and diminished air quality) at both local and regional levels [2,6–9]. Such UHI related impacts are also called UHI regional impacts (UHIRIP). Generally, UHI research includes data from two major sources: air temperature data that are observed by weather or climate stations and remotely sensed data to observe UHI through land surface temperature. Before the availability of remotely sensed data, UHI was widely observed in the field, with the first scientific observation of UHI in 1833 [10]. Field observations of UHI continue to be a critical source of training and validation data [11,12]. These observations, along with modeling studies, continue to help unravel the factors that are responsible for UHI development, and are providing a basis for the development and application of sustainable adaptation strategies. Communicating scientific knowledge quickly and effectively of UHI and UHIRIP to architects, engineers, scientists, and planners could help inform urban

design and decision making. Remotely sensed data have been used to observe UHI and UHIRIP on environments, ecosystems, human health, and economics in urban and non-urban areas for decades. Remote sensing offers the benefits of long data archives, repeated observations, efficiency, and multiple temporal and spatial resolutions. UHI studies using remotely sensed data have been published for hundreds of cities worldwide [6,7,13–19]. Remotely sensed data provide highly efficient, long-term, and broad-scale information for assessing UHIRIP. However, studies integrating high spatial resolution imagery (e.g., Landsat at 30 × 30 m and ECOSTRESS at 70 × 70 m) from multiple sensors to evaluate UHI and UHIRIP across a time series have been uncommon. Challenges to such studies include image frequency and calibration, cloud contamination, and the need for large storage and high-performance computing capabilities [20,21]. Early generations of broad-scale UHI assessment using remote sensing often poorly represented the spatial and temporal variance in UHI, especially at the urban and non-urban interface. As the resolution of algorithms and satellite imagery improved and interest in UHIRIP grew, researchers sought better representations of UHI. Initially, this took the form of modifications based on surface physical characteristics such as roughness length, albedo, thermal conductivity, and thermal diffusivity [22,23]. Many studies have been conducted to understand the urban thermal climate or the potential for heat island mitigation using this framework of simplified algorithms [24–26]. In more recent efforts, researchers have incorporated more sophisticated parameterization schemes that have included distributions of demography, policies, and behavior of government; ecological variables and ecosystem services; land use and land cover change (LULCC) patterns; and social and economic factors to represent the complicated impacts of UHI [27–36].

Historically, the study of UHI using remote sensing data, often Landsat data, was mainly based on comparing images at two different times using the bitemporal approach [37–39]. Although the bitemporal approach is mathematically simple and does not need large amounts of data, it is less useful than a time series approach that is able to provide a more comprehensive understanding of the complexity of UHI. Most early research [17,40–42] in UHI focused on cities or urban areas, and often ignored the urban and non-urban interface at regional scales. In recent decades, the cost of data storage has dramatically decreased, and we have witnessed an overwhelming increase in computing power and open source software that provide the foundations for time series analysis using higher resolution thermal data from satellite archives. Some studies used Landsat time series to detect historical changes [20,43–46], but few have focused on UHI and its interaction with land use and land cover (LULC) dynamics. A research team at the USGS Earth Resources Observation and Science (EROS) Center recently developed the Land Change Monitoring, Assessment, and Projection (LCMAP) project [47], which is produced with Landsat Analysis Ready Data (ARD) [48] and land surface temperature (LST) data. LCMAP data provide the potential to use Landsat LST data to analyze UHI in urban agglomerations, as well as the urban and non-urban interface at local, regional, and global scales.

This paper reviews remote sensing thermal data sources and the most up-to-date methods used for UHI and UHIRIP investigations. We start by defining UHI, UHII (UHI intensity), regional impacts, urban and non-urban interface, and remotely sensed data sources for LST. We then describe the major distinct approaches that have been used to estimate the magnitude, spatial distribution, intensity, and change pattern of UHIRIP in urban agglomerations and at different urban and non-urban interfaces. Our primary goals in this review are to describe (1) a brief historical summary in the research of UHI and UHIRIP, (2) major thermal data sources and methods used in UHI and UHIRIP research, (3) algorithms used in UHI and UHIRIP analysis, and (4) future research perspective and potential direction. Following the introduction, we discuss the development of UHI and UHIRIP in Section 2; in Section 3, we focus on the application of the remotely sensed thermal datasets in UHI and UHIRIP; we review the algorithms for UHI and UHIRIP in urban and non-urban interface studies based on remotely sensed data in Section 4; in

Section 5, we summarize UHI and UHIRIP based on remotely sensed data; and in Section 6, future research directions are discussed.

2. Development of UHI and UHIRIP Analysis

Most satellite-based investigations of UHIs can be summarized into five main objectives: (1) to examine the spatial features of urban thermal patterns and change dynamics and their relations to urban surface characteristics; (2) to study urban surface energy balances through coupling with urban climate models, including simulation and projection; (3) to study the relations between atmospheric heat islands and surface UHIs through combining coincident remote and ground-based observations; (4) to develop approaches to reduce the magnitude of the UHI and its regional impacts; and (5) to study the UHI effects on ecosystem security at a regional level. Several important reviews, bibliographies, and summaries on UHIRIP using remotely sensed data have been published (see list and descriptions in Table 1). These reviews have concentrated mostly on the various worldwide perspectives of UHI, including the definition of fundamental concepts, summary of methods, applications, exploration of output characteristics, outlines of key research findings, and potential future directions (Tables 2 and 3). The focus of this paper is on the algorithms and methods used in studies employing remote sensing thermal data for UHI and UHIRIP investigation, and future directions in this realm. We summarize (1) the disadvantages of using limited time remotely sensed data for UHI and UHIRIP analysis; (2) the limitations of data shortages due to cloud cover and satellite revisit intervals; (3) the applications of gap filling, data fusion, and deep learning; and (4) the trade-offs between high temporal frequency data (MODIS) and high spatial resolution (Landsat) time series.

Table 1. Example of main reviews, bibliographies, and summaries on UHI and UHIRIP using remotely sensed data.

Reference	Topics	Sensors	Measurements
Hall et al. [11]	Satellite remote sensing of surface energy balance success, failures, and unresolved issues in field experiment (FIFE)	Landsat, SPOT	Thermal
Gallo et al. [13]	Assessment of urban heat islands: A satellite perspective	AVHRR, Landsat MSS	Thermal
Voogt and Oke [6]	Thermal remote sensing of urban climates	Multiple, review	Thermal
Weng and Larson [49]	Satellite remote sensing of urban heat islands: current practice and prospects	Multiple, review	Thermal
Jiang et al. [50]	Land surface emissivity retrieval from combined mid-infrared and thermal infrared data of MSG-SEVIRI	Meteosat Second Generation (MSG)	Spinning Enhanced Visible and Infrared Imager (SEVIRI)
Kalma et al. [51]	Estimating land surface evaporation: A review of methods using remotely sensed surface temperature data	Multiple, review	Thermal
Racoviteanu et al. [52]	Optical remote sensing of glacier characteristics: a review focusing on the Himalaya	ASTER	Indices
Rizwan et al. [53]	A review on the generation, determination, and mitigation of urban heat island	Review	Determination of UHI
Weng [7]	Thermal infrared remote sensing for urban climate and environmental studies: Methods, applications, and trends	Multiple, review	Thermal
Bowler et al. [31]	Urban greening to cool towns and cities: A systematic review of the empirical evidence	Review	Synthesis analysis
Sailor [54]	A review of methods for estimating anthropogenic heat and moisture emissions in the urban environment	Review	Bibliometric profile
Li et al. [55]	Satellite-derived land surface temperature: current status and perspectives	Multiple, review	Thermal

Table 1. *Cont.*

Reference	Topics	Sensors	Measurements
Ngie et al. [56]	Assessment of urban heat island using satellite remotely sensed imagery: A review	Multiple, review	Thermal
Rasul et al. [16]	A review of remote sensing of urban heat and cool islands	Multiple, review	Thermal
Huang and Lu [57]	Urban heat island research from 1991 to 2015: A bibliometric analysis	Review	Bibliometric profile
Zhang et al. [58]	A bibliometric profile of the remote sensing open access journal published by MDPI between 2009 and 2018	Multiple, review	Bibliometric profile
Deilami et al. [59]	Urban heat island effect: A systematic review of spatio-temporal factors, data, methods, and mitigation measures	Multiple, review	Thermal
Zhou et al. [60]	Satellite remote sensing of surface urban heat islands: Progress, challenges, and perspectives	Multiple, review	Thermal
Becker and Zhao-Liang [61]	Surface temperature and emissivity at various scales: definition, measurement, and related problems	Multiple, review	Thermal (surface temperature and emissivity)
Dash et al. [62]	Land surface temperature and emissivity estimation from passive sensor data: theory and practice current trends	Multiple, review	Thermal (surface temperature and emissivity)

Table 2. Examples of research publications investigating UHI and UHIRIP using remotely sensed data.

UHI Applications	Example of Research
Classification with LST, index, albedo	Miles and Esau [63], Trlica et al. [64], Bonafoni [65], Wong and Nichol [66], Jin [67], Wu et al. [68], and Hu and Brunsell [69]
Regression models, geostatistical analysis	Zhang and Du [70], Wicki and Parlow [71], Dai et al. [72], Song et al. [73], Sellers et al. [74], Du et al. [75], Shahraiyni et al. [76], Chun and Guldmann [77], Ho et al. [78], and Lai et al. [79]
Multiple sensors, data fusion	Huang and Wang [80], Li et al. [81], Berger et al. [82], Liu et al. [83], Fu and Weng [84], Liang and Weng [85], and Dousset and Gourmelon [86]
Machine learning, decision support information system	Chakraborty and Lee [87], Mpakairia and Muvengwi [88], Zhang et al. [89], Tran et al. [90], Shahraiyni et al. [76], Weng and Fu [91], Mallick et al. [92], Connors et al. [93], Wentz et al. [94], Xian and Crane [95], Wilson et al. [96], and Xian et al. [97]

Table 3. The temporal frequency and spatial resolution of the main remotely sensed thermal data.

Sensor	Temporal Frequency (day)	Spatial Resolution (m)
Landsat 5 TM	16	120 (resampled to 30)
Landsat 7 ETM+	16	60 (resampled to 30)
Landsat 8 TIRS	16	100 (resampled to 30)
Terra ASTER	15	90
Terra MODIS	1	1000
Aqua MODIS	1	1000
NOAA-AVHRR	1	1000
VIIRS	1	750
ECOSTRESS	Various (randomly, 0.5)	70

2.1. Urban Heat Island

UHI studies have been conducted for over 200 years, since the first conceptualization by Luke Howard in 1818 [98]. Generally, an urban heat island (UHI) is an urban area or metropolitan area that is significantly warmer than its surrounding rural areas because of human activities. The temperature difference is usually greater at night than during the day and is most apparent when winds are weak. Some research [99,100] shows that the annual mean air temperature of a city with 1 million people or more can be 1–3 °C warmer than its surroundings. In the evening, the difference can be as high as 12 °C. Heat islands can affect

communities by increasing the summertime peak energy demand (such as air conditioning costs), air pollution and greenhouse gas emissions, heat-related illness, and mortality, and decreasing water quality and ecosystem security. Higher temperature "domes" are created over an urban or industrial areas by hot air layers forming at building-top or chimney-top level. This dome is about 5 °C to 7 °C warmer than the air above it and the ground level temperature, and can trap all polluting emissions within its confines (see also temperature inversion [53,57]).

The large amount of heat generated from urban structures and pavements, as they absorb and re-radiate solar radiation, as well as the heat from other anthropogenic sources, are the main causes of UHI. These heat sources increase the temperatures of an urban area compared with its surroundings, which is known as UHI intensity (UHII). Traditionally, regardless of the methodology employed, whether it refers to (1) differences between two fixed observatories, one urban and another peripheral or non-urban; (2) mobile urban transects; or (3) remote sensing analysis, UHII provides a value of thermal differences between contrasted points, sectors, or areas, one urban and another that could be termed non-urban. Thus, the intensity of the UHI is seen in the temperature difference expressed at a given time between the hottest sector (areas) of the city and the surrounding non-urban space. The intensity of the heat island is the simplest and most quantitative indicator of the thermal modification imposed by the city upon the territory in which it is situated and of its relative warming in relation to the surrounding rural environment. The intensity could be defined for various time scales and geographical locations [101,102].

2.2. The Study of the Spatial Structure of Urban Thermal Patterns, Change Dynamics, and Their Relation to Urban Surface Characteristics

Based on the fractional theory of ecology [103,104], the spatial structure of urban thermal patterns and temporal change dynamics can be studied in two and three dimensions. Figure 1 shows an example of the UHI and UHIRIP profile in Sioux Falls, South Dakota, USA, and the surrounding area, derived from Landsat ARD LST over different land cover classes [97]. The study of temporal change in UHI can include multiple scales of change, including daily, day and night, monthly, seasonal, yearly, and long-term time series. The physical mechanisms driving UHI are well documented [28]. UHIRIP may be described in multiple ways with various methodological approaches to investigate each type; specifically, it can impact the ground, the surface, and various heights in the air [105,106] at a regional scale. Different pictures arise for each type of UHI when measured by different methods. Tam et al. [107] suggested that the magnitude of total change in day to day temperature variability can be used to decide a suitable urban/rural pair for any urbanization impact study. Generally, the UHI at a regional scale is best measured using remotely sensed data with one or multiple thermal bands. When explaining the character of remotely sensed UHI, Roth et al. [108] assert, "satellite-derived surface heat islands are in a separate class and it is not clear that they will match others measured by more conventional means in the urban canopy layer or the urban boundary layer". Their precautionary statement relates in part to the surface "seen" by remote sensing platforms that depend on altitude and the camera or sensor angle. Imagery collected at nadir and/or high altitude primarily consists of rooftops, streets, crop fields, and vegetation canopies. Observations from lower heights at oblique angles consist of items seen from a bird's-eye perspective plus varying degrees of vertical features in the landscape, such as the walls of buildings. As a result, angle can have a large influence on the urban surface temperatures recorded by airborne and spaceborne thermal infrared sensors [109]. Another concern regards mixed pixels (i.e., individual pixels containing surfaces having different physical properties, depending on the spatial resolution of the data), which can complicate image analysis. This is especially true for thermal sensors aboard satellites, because most have a spatial resolution that is coarser than the other spectral bands on the satellite. The typical variation of urban surface properties also complicates thermal sensors. A final consideration when using remotely sensed imagery involves correcting for atmospheric attenuation. For many applications, these issues are far outweighed by remote sensing's

benefits. With high spatial resolution thermal data, these issues can typically be resolved. Additionally, from a macro research perspective, remotely sensed thermal data have the major advantage of investigating UHI and UHIRIP at a broad scale, permitting focus on environmental issues in urban agglomerations and surrounding areas, and at urban and non-urban interfaces.

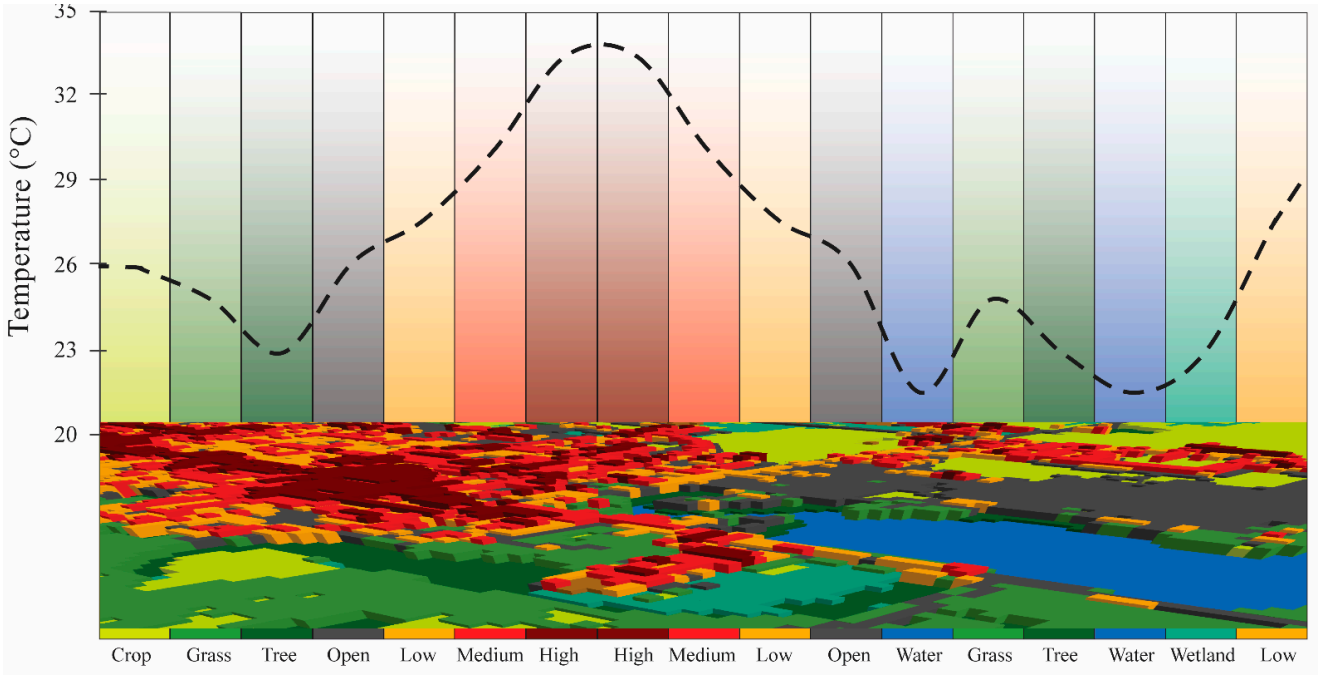

Figure 1. An example of UHI and UHIRIP in the urban and the urban and non-urban interface for part of the Sioux Falls, SD area.

2.3. Simulation and Projection of UHI and UHIRIP

Applying theories of landscape ecology [104], UHI studies focus on moving from static spatial structures of urban thermal patterns to the change dynamic of spatial patterns and processes of urban thermal characteristics. The spatial structure of UHI patterns determines the processes of UHI impacts. Li et al. [110] simulated the urban climate of various generated cities under the same weather conditions. By studying various city shapes, they generalized and proposed a reduced form to estimate UHI intensities based only on the structure of urban sites, as well as their relative distances. They concluded that in addition to the size, the UHI intensity of a city is directly related to the density and the amplifying effect that urban sites have on each other. Their approach can serve as a UHI rule of thumb for the comparison of urban development scenarios. Ramírez-Aguilar and Lucas Souza [111] present a study based on the relationship between UHI and population size (p) by considering the population density (PD) and the urban form parameters of different neighborhoods in the city of Bogotá, Colombia. They concluded that urban form, expressed by land cover and urban morphology changes caused by population density, has a great effect on temperature differences within a city. Advances in computing technology have fostered the development of new and powerful deep learning techniques that have demonstrated promising results in a wide range of applications. In particular, deep learning methods have been successfully used to classify remotely sensed data collected by Earth observation instruments [112]. Deep learning algorithms, which learn the representative and discriminative features in a hierarchical manner from the data, have recently become a hotspot in the machine-learning area, and have been introduced into the geoscience and remote sensing community for remotely sensed big data analysis [113]. With climate change, the simulation and projection of UHI and its regional impact by using computer

technology (deep learning) and remotely sensed data are becoming more important for urban planning and policy makers.

2.4. Challenges for Land Surface Temperature and Emissivity Retrieval (Separation)

Land surface temperature and emissivity are two important surface parameters that can be derived from remotely sensed data after atmospheric correction [114–116]. Besides radiometric calibration and cloud detection, two main problems need to be resolved in order to obtain land surface temperature and emissivity values from various satellite sensors. These problems are often referred to as land surface temperature and emissivity separation (TES) from radiance at ground level, and as atmospheric corrections in the literature [117,118]. Reliable retrieval of urban and intra-urban thermal characteristics using satellite thermal data depends on accurate removal of the effects of atmospheric attenuations, as well as angular and land surface emissivity. In the thermal infrared of remotely sensed data, the emission of the targets is dominant when compared with the reflection, and this radiation is a function of two unknowns—the emissivity and the temperature of the target [119]. The temperature and emissivity separation is complex because of the existing non-linear relationship between temperature and radiance. The complex dynamics of these relationships within the target (atomic level) propagates in a cascade effect, reflecting variations in determining emissivity. Mohamed et al. [117] reviewed details of LST and land surface emissivity (LSE) retrieval methods and their potential for adoption in medium spatial resolution, including ASTER and Landsat. The review further comments on spatial and temporal prospects of effective intra-urban surface thermal mapping. They also suggested future development of land surface temperature and emissivity estimation for UHI assessment. Li et al. [120] described the theoretical basis of LSE measurements and reviewed the published methods. They also categorized these methods into (1) (semi-) empirical or theoretical methods, (2) multi-channel temperature emissivity separation (TES) methods, and (3) physically based methods (PBMs). Then, they discussed the validation methods that are important for verifying the uncertainty and accuracy of retrieved emissivity. Finally, the prospects for further developments are given. These studies provided a forum for assessing what had been achieved by the UHI community over four decades, and what needs to be done in the near future. It is clear that the observation, experiments, and algorithm development efforts, although completely worthwhile for scientists, need to deliver various datasets, especially from remotely sensed data to modelers working in the areas of UHI and UHIRIP at local, regional, and global levels. A lot of basic theoretical research and scientific verification work has been done on scale issues, as well as scaling issues including emissivity and temperature measurements related to remote sensing standards [121]. All of the methods described in Rolim et al. [119] represent the largest and main part of the existing methods of temperature and emissivity separation developed in the last four decades, but further research is necessary for more precise methods that are less susceptible to errors during the separation of these variables.

2.5. The Relationship between Atmospheric Heat Islands and Surface UHI through Combining Coincident Remote Sensing and Ground-Based Observations

Generally, UHI data are obtained from one of two sources—weather stations and remote sensing. Remotely sensed data have been used to observe how UHI impacts climate change in urban and non-urban areas for decades because of the multiple temporal and spatial resolutions of remotely sensed datasets. Hundreds of published studies explore UHI and its impacts by using these two data sources, but the relationship between air temperature obtained from field stations and surface temperature derived from remote sensing remains unclear. Wang et al. [122] investigated the relationship of canopy UHI (CUHI) and surface UHI (SUHI) using four observations per day, without temporal averaging, in four different cities in two different global regions, with 201 of 2232 CUHI–SUHI pairs exhibiting significant UHI differences in their spatial distributions and intensities. The results indicate that 81.09% of the UHI differences occurred during the daytime and were caused by local air advection related to wind speed $\geq$2 m/s and land surface conditions

in the study areas. They concluded that a joint analysis of CUHIs and SUHIs should be conducted to characterize urban thermal environments, and that current urban planning procedures should integrate these UHI differences to develop effective mitigation strategies and adaptation measures. The combination of both types of UHI sub-components provides added value for quantifying urban thermal environments, which can assist in developing effective mitigation strategies and adaptation measures. A growing trend is to combine the two methods, both with their own advantages [59].

2.6. Develop Controlling Approaches for UHI and UHIRIP

UHIs occur when cities replace other land covers with dense concentrations of pavement, buildings, and other surfaces that absorb and retain heat. This effect increases energy costs (e.g., for air conditioning), air pollution levels, and heat-related illness and mortality. UHI results from increases in built-up surfaces in urban areas, whereas increasing vegetation cover and water surfaces within cities or urban agglomerations could improve the urban ecological function and thereby improve urban environments for humans [123]. The importance of optimizing urban LULC planning and the development of UHI mitigation methods is increasing. Progress has been made to this end [67,124,125], with the development of UHI mitigating technologies [126]. Ulpiani et al. [127] reviewed an infrared emissivity dynamic switch against overcooling, which is aimed at collecting state-of-the-art technologies and techniques to dynamically control the heat transfer to and from the radiative emitter and to ultimately modulate its cooling capacity using spacecraft thermal control, thermal camouflage, and electronics. This work discussed prominent pathways toward technically and economically effective integration in the built environment for UHI and UHIRIP.

2.7. UHI and UHIRIP on Socioeconomics and the Urban Ecosystem

2.7.1. Impacts on Human Health

Climate change, increasing urbanization, and an aging population in much of the world are likely to increase the risks to health from UHI, particularly from heat exposure. Additionally, increased urbanization has resulted in a more extensive UHI effects, causing more frequent and intense heat waves in urban regions compared with rural locales [67,128,129]. In urban and surrounding areas, heat waves will be exacerbated by the UHI effect and will have the potential to negatively influence the health and welfare of residents. Heaviside et al. [130] suggest that UHI contributed around 50% of the total heat-related mortality during the 2003 heat wave in the West Midlands of the UK. Moon [131] concluded that the mortality and morbidity risks of diabetic patients under the heat wave were mildly increased by about 18% for mortality and 10% for overall morbidity. Li et al. [132] found that high temperature significantly increases the risk of mortality in the population of Jinan, China. Most research in this topic uses both weather station and in situ measurements in order to investigate the health effects of UHI [129]. Some results [133] show that different sites (city center or surroundings) have experienced different degrees of warming as a result of increasing urbanization [131]. Johnson et al. [134] suggest that thermal remote sensing data can be utilized to improve the understanding of intra-urban variations of risk from extreme heat. The refinement of the current risk assessment systems could increase the likelihood of survival during extreme heat events and assist emergency personnel in the delivery of vital resources during such disasters. The conclusion is that UHI is directly linked to adverse health effects from exposure to extreme thermal conditions.

2.7.2. UHI and UHIRIP on LULC Differences and Change

UHI is a result of continued urbanization, urban agglomeration, and associated increases in paved areas and buildings. Mitigation strategies have been developed to increase vegetation and water surface areas within urban areas to reduce the magnitude of the temperature. One measure of UHI's ecological footprint is estimated by calculating the

increase of the cooling demand caused by the heat island over the urban area, and then translating the increased energy use to environmental cost [123,125,135]. Some research shows that the UHI effect has become more prominent in areas of rapid urbanization and in urban agglomerations [136,137]. The spatial distribution of UHI has changed from a mixed pattern, where bare land, semi-bare land, and land under development were warmer than other LULC types, to extensive UHI, as contiguous urbanized blocks grew larger [38,138]. Some analyses showed that the higher temperature in the UHI had a scattered pattern and was related to certain LULC types [97]. In order to analyze the relationship between UHI and LULC changes, some studies attempted to employ a quantitative approach for exploring the relationship between surface temperature and several indices, including the Normalized Difference Vegetation Index (NDVI), Normalized Difference Water Index (NDWI), Normalized Difference Bareness Index (NDBaI), and Normalized Difference Build-up Index (NDBI). It was found that correlations between NDVI, NDWI, NDBI, and temperature are negative when NDVI and NDWI are limited in range, but there is a positive correlation between NDBI and temperature [139–142].

2.7.3. Impacts on Regional Economics

Because UHI is related to a significant increase in surface temperature and changes in precipitation patterns, it can potentially affect local economies and the social systems of cities [143]. Some studies [144,145] show that the critical sectors of services, agriculture, and tourism may be strongly affected by future UHIs. To counterbalance the consequences of the increased urban surface temperatures, important research has been carried out resulting in the development of efficient mitigation technologies. In particular, some studies [102,146] have documented the development of highly reflective materials, cool and green roofs, cool pavements, urban greens, water surface, and other mitigation technologies. UHIRIP includes economic impacts, such as increases of energy consumption for cooling purposes, as well as an increase in the peak electricity load, which is a factor for planning maximum power source capacities [147]. Scientists from Australia reported that the total economic cost to the community due to hot weather is estimated to be approximately $1.8 billion in present value terms. Approximately one-third of these impacts are due to heat waves. Of the total heat impact, the UHI effect contributes approximately $300 million (AUD) in present value terms for the city of Melbourne, Australia [9]. Estrada, Botzen and Tol [144] provided a quantitative assessment of the economic costs of the joint impacts of local and global climate change for all main cities around the world. They estimated the UHI effect for the 1692 largest cities in the world for the period 1950–2015, and predicted that the percentage of city gross domestic product (GDP) that would be lost for the median city in 2050 due to global climate change alone would be relatively small: 0.9% and 0.7% for the RCP8.5 and RCP4.5 emission scenarios, respectively [144]. At the end of the century, these impacts will increase to 3.9% and 1.2%, respectively. Cost–benefit analyses are presented of urban heat island mitigation options, including green and cool roofs and cool pavements. It has been shown that local actions can be climate risk-reduction instruments. Furthermore, limiting the urban heat island through city adaptation plans can substantially amplify the benefits of international mitigation efforts.

2.7.4. Impact on Biodiversity

Besides UHI, urban development causes wildlife habitat loss and fragmentation, threatens wildlife populations, increases fire risk, and reduces biodiversity [2,148]. These problems are of particular concern in the wildland urban interface (WUI), where homes and associated structures are built among forests, shrublands, or grasslands [1,148,149]. The WUI has received considerable attention because of recent increases in both the number of structures destroyed and the area burned annually by wildland fire. Čeplová et al. [150] studied three habitats with different disturbance regimes in 45 central European settlements of three different sizes. Their results highlight the importance of urban size as a factor shaping the biodiversity of native and alien plant communities in individual urban habitats,

and the important role of habitat mosaic for maintaining high species richness in city floras. The study of Coluzzi et al. [151] represented a first step to improve the description of relevant processes to protect natural habitats and quality agriculture, therefore combating land degradation and detrimental climate change effects. Kaiser et al. [152] monitored temperature and relative air humidity in wooded sites characterized by different levels of urbanization in the surroundings, and investigated the effect of urbanization at the local and landscape scale on two key traits of biological fitness in two closely related butterfly species that differ in thermal sensitivity.

3. Remotely Sensed Thermal Datasets

Remote sensing derived LST is effective for UHI and UHIRIP studies. Satellites can quickly obtain continuous information over a large geographic area that can be maintained in long-term archives. LST for large geographic areas can be derived from surface radiation of heat measured by satellite sensors. This is particularly attractive when investigating the surface UHI in multiple cities or urban agglomerations at various spatial extents. Along with the extensive spatial coverage, many satellites record multiple wavelengths of electromagnetic energy that can be used to decipher a wealth of information, in addition to thermal information (Figure 2). Consequently, multispectral imagery allows for a comparative analysis between LST and other variables, such as land cover and vegetation indexes [50,153], specifically the interaction between UHI and LULCC [154]. Remote sensing can also be used to track the patterns of change in UHI over time through various time periods from a day, to years, and even a time series of decades [38,155–158]. Because information is desired at a high spatial resolution and dense temporal frequency, data from multiple sensors can make more accurate and reliable quantitative assessments of UHIRIP studies [60]. Table 3 includes a list of the main remotely sensed datasets that have been recently used to derive LST and analyze UHI and UHIRIP.

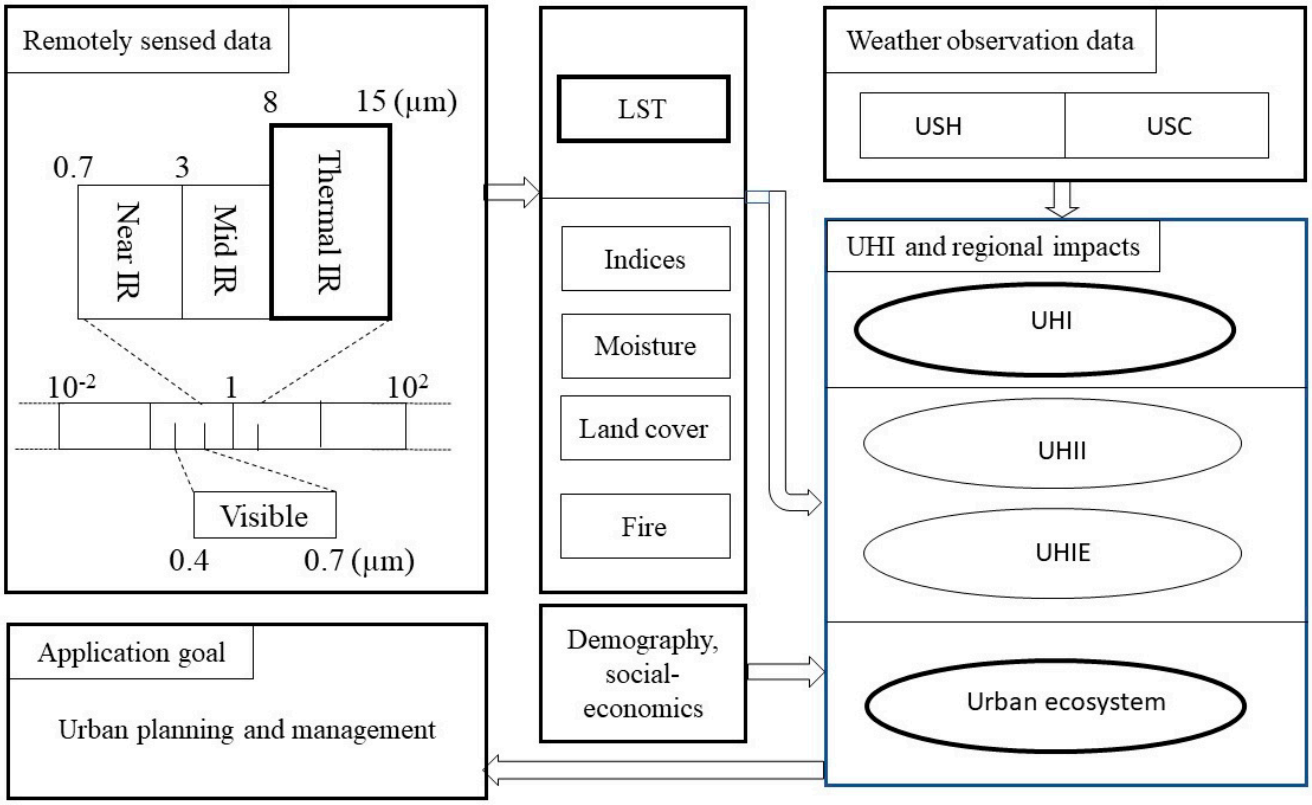

Figure 2. Schematic diagram for using remotely sensed data to evaluate UHI and UHIRIP. Bold outlines indicate high importance. USH—US historical weather data; USC—US climate data; UHI—urban heat island; UHII—UHI intensity; UHIE—UHI effects; IR—infrared band.

The rapid development of remote sensing technology offers more potential for accurate and reliable quantitative assessments of UHI (Table 3 and Figure 3). Many researchers (Table 2) have used remotely sensed LST to assess UHI over various geographic areas. However, for all of these studies, the 1 × 1 km spatial resolution of coarse datasets was found to be suitable only for broad-scale urban temperature mapping (Table 4). The higher resolution of Landsat time series is suitable for UHIRIP at various scales (Table 4).

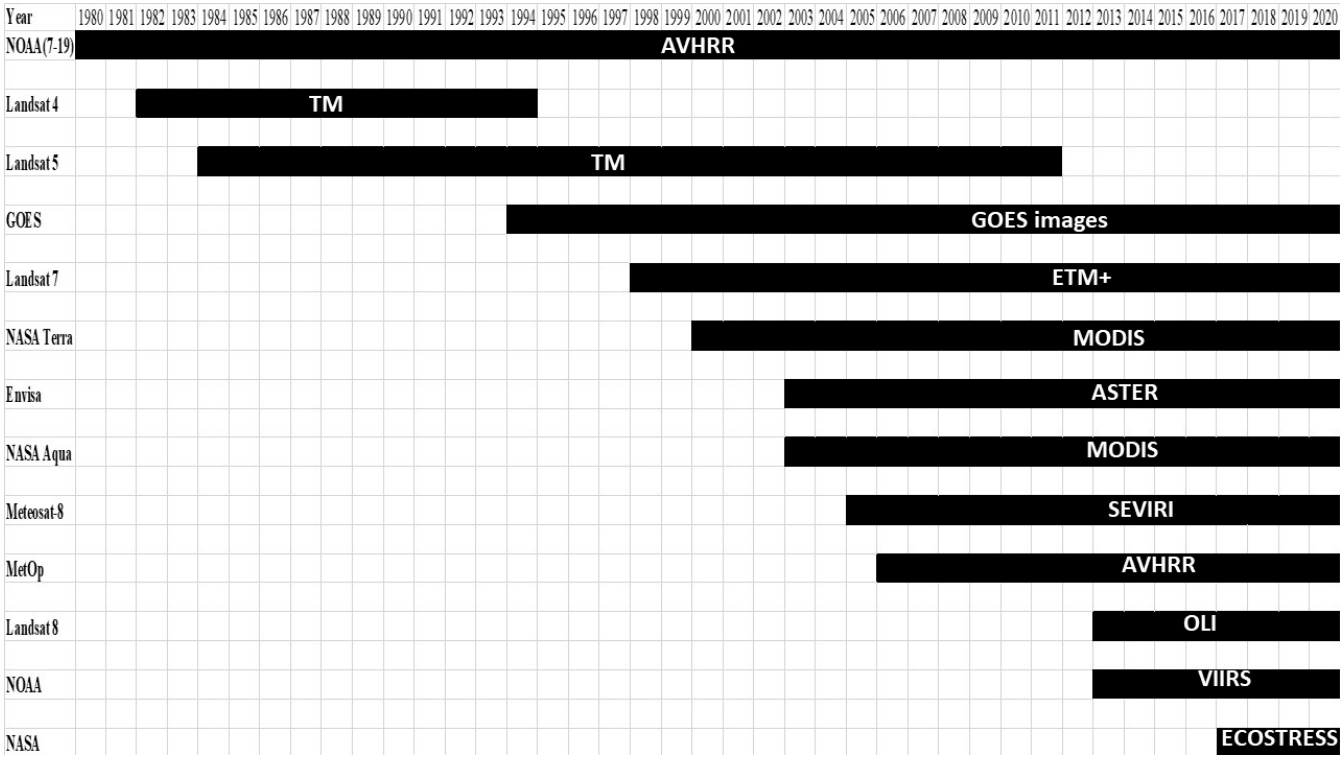

Figure 3. Timeline of satellite data availability. Data availability to 2020 indicates ongoing availability.

Table 4. Proportion of reviewed UHI, UHII, and UHIE studies using various remotely sensed data.

Sensor	%	Examples
Airborne	<1%	Liu et al. [159], and Ben-Dor and Saaroni [160]
AVHRR	4%	Stathopoulou and Cartalis [161], and Gallo and Owen [162]
MODIS	24%	French and Inamdar [115], Zhi Qiao et al. [163], and Keramitsoglou et al. [164]
ASTER	6%	Gillespie et al. [118], Ye et al. [165], Kato and Yamaguchi [166], and Lu and Weng [167]
VIIRS	<1%	Sun et al. [168], Quan et al. [169], and Gawuc and Struzewska [170]
Landsat Series	52%	Aniello et al. [171], Weng [172], Stathopoulou and Cartalis [173], and Sagris and Sepp [174]
ECOSTRESS	<1%	Hulley et al. [175] and Schultz et al. [176]
Multiple sensors	8%	Dousset and Gourmelon [86], and Elmes et al. [177]
Others	<1%	Huang and Wang [80]

Voogt and Oke [6], and others [156,178] pointed out that improved spatial and spectral resolution of sensors and advances in digital image processing techniques increase the usefulness of remote sensing for UHI and UHIRIP studies. Forster [179] also stated that satellite, radar, and airborne sensors can provide spatially continuous information pertaining to numerous variables in urban environments that complement field observations. An increasing number of studies directly relate remotely sensed data to in situ field data [180,181], and applications of remote sensing technology will expand UHI studies to various geographic extents. An exciting recent trend in UHI and UHIRIP research involves

coupling remotely sensed data with ancillary and social economic datasets from multiple sources (Table 2). The typical examples include (1) fractional vegetation cover derived from satellite data to improve model simulations of UHI [182], (2) incorporation of remotely sensed data into a model that partitioned various fluxes in the surface energy balance [183], (3) integrating high-resolution multispectral data with property tax records to investigate the contribution of residential land use to UHI formation [184], (4) studying the potential application of change in urban green space as an indicator of urban environmental quality change [185], (5) using parameters from thermal satellite data and three-dimensional virtual reality models to better understand the factors controlling urban environmental quality (UEQ) [186], (6) further advancing the use of remotely sensed imagery to evaluate UEQ by estimating ground-level particulate matter (PM) concentrations using satellite-based data [187], and (7) estimating the value of U.S. urban tree cover for reducing heat-related health impacts and electricity consumption [188]. In addition, NASA's Ecosystem Spaceborne Thermal Radiometer Experiment on the International Space Station (ECOSTRESS) was launched in June 2018, and is able to image fine-scale temperatures in cities at a 70 × 70 m resolution throughout different times of the day, every 3–5 days on average, over most of the globe [146]. With new algorithm development, ECOSTRESS can accurately monitor UHI trends over time in vulnerable areas such as the urban and non-urban interface. With more available remotely sensed data (Figure 3), innovative studies like these hint at the potential for remote sensing to play an even more prominent role in research of urban climate, urban environment, urban ecological service, and urban planning in the future.

4. Algorithms for UHI and UHIRIP in Urban and Non-Urban Interface Studies Based on Remotely Sensed Data

Generally, the methods for evaluating UHI and UHIRIP can be summarized into four basic types: (1) historical weather station data, (2) field observation, (3) computer simulation, and (4) remote sensing technology. The limitations of the first three methods have been well documented [53,57,105,180]. In this paper, we only focus on the methods that use remote sensing technology. A number of algorithms (or methods) have been developed to estimate UHI and UHIRIP from remotely sensed data (Table 5), including simple empirical approaches to complex methods based on remotely sensed data assimilation using various models. The structure of the UHIRIP pattern centroid in three dimensions indicates the overall variation of the intensity and distribution of the UHI in space and time. The simplified relationship of thermal data and UHI has been applied from a local spatial scale using airborne very high-resolution images to a broad scale with AVHRR, MODIS, ASTER, and Landsat data at regional and continental levels. Assimilation procedures of UHI often require remotely sensed data over different spectral domains to retrieve input parameters that characterize surface properties such as thermal properties, albedo, NDVI, and other indices. A brief review of these approaches is presented in Table 5, with a discussion about the main physical bases and assumptions of various models.

Detailed knowledge of UHI and UHIRIP, especially latent and sensible heat flux components, is important for monitoring the climate change of the land surface. The main methods classically used to measure UHI are appropriate to field observations [24–26,189], but do not allow for an estimation of UHI at large spatial scales. For operational applications to ecological conservation and city planning, managers and engineers need accurate estimates of land surface temperature and UHI at broad spatial scales. New algorithms based on remotely sensed data have been developed to use the imagery of various spatial resolutions and temporal frequency to evaluate UHI [190–192]. It is often difficult to classify these methods because their complexity depends on the balance between the empirical- and physical-based modules used. Nevertheless, we summarize some algorithm (model) categories in the following subsection.

Table 5. Methods used to measure UHI and UHIRIP using remotely sensed data.

Method	Sensor	Period	Example
Calculate LST	All thermal bands	1970s–current	Avdan and Jovanovska [193], and Peng et al. [194]
Determine the UHIE	Landsat	2009	Tang et al. [195]
Determine the UHII	MODIS	2001, 2003	Tran et. al. [156]
Compare multi-temporal LST images	The normalization of the temperature based on the mean and standard deviation in high and low temperature areas.		Streutker [39]
	Common normalization of temperture based on min and max LST of the same image in the same way as for NDVI. A normalized ratio scale technique.		Chen et al. [38]
Statistical analyses of UHI	The relationship between LST, NDVI, ground vegetation (GV), and impervious surface area (ISA). Multiple linear regression. Geographically weighted regression.		Weng et al. [153], Tran et al. [156], Schwarz et al. [196], Szymanowski and Kryza [197], and Firozjaei et al. [198]
	A support vector machine regression (SVR) mode. LST	2012 (daily)	Lai et al. [79]
Data fusion	Landsat, MODIS	1988–2013,	Shen et al. [192], Wengand Fu [17], and Schmitt and Zhu [199]
Gap filling	Landsat	2020	Yan and Roy [178], Zhou et al. [60], Fu et al. [190], and Zhou et al. [200]
Time-series analysis	Landsat	1984–2015	Huang et al. [201], Peres et al. [202], Fu and Weng [203], and Xian et al. [97]
Uncertainty and accuracy assessment	MODIS, Landsat		Shen et al. [192], Lee et al. [204], Yuan and Bauer [205], and Chen et al. [206]

4.1. LST and UHI Intensity Calculation

LST calculation, including empirical direct methods where remotely sensed data are introduced directly in semi-empirical models to estimate LST, is the simplified relationship between thermal infrared remotely sensed and meteorological data [14]. This method allows for the characterization of UHI intensity both at the local scale, using ground measurements, and over large areas, using satellite data, by calculating a cumulative temperature difference [55,92]. Most current operational models [60] use remote sensing directly to estimate the input parameters and LST.

Seasonal information captures the annual profile of LST and its trend over long time periods, and is essential to the study of UHI [207]. Therefore, remote sensing has been used to accurately monitor and compare the LST difference in the same season in different years and trends over long time periods. In the last 10–15 years, thermal sensor technology has been rapidly developing (Figure 3). Three types of methods have been developed to estimate LST with remotely sensed data: the single infrared channel method; the split window method; and a new day–night MODIS LST method, which is designed to take advantage of the unique capability of the MODIS instrument [55]. Recently, Peng et al. [194] proposed a wavelet coherence approach to exploring spatial heterogeneity and the scale-dependence of the relationship between LST and multiple influencing factors. The advantages, disadvantages, and applicability of these three types of algorithms are summarized in Table 6.

Table 6. Advantages, disadvantages, and applicability of commonly used algorithms for calculating LST.

Type	Algorithm	Advantages	Disadvantages	Example
Single window	Atmosphere correction	LST for oasis in arid lands	Complicated, errors, only use for one band thermal	Landsat TM/ETM+, CBERS/IRMSS
	Qin Sing window	Accurate and applicable	Need three atmosphere parameters, only use for one band thermal	
	Universal single channel	Do not need atmosphere parameters, applicable for multiple sensors	The result impacted by standard atmosphere	
Split window	NOAA-AVHRR	Most used, accurate, applicable for most sensors, less requirement of parameters, simple models	Not accurate LST in mixed pixels	NOAA/AVHRR3 TERRA/MODIS Landsat 8/TIRS
	TERRA-MODIS			
	Landsat-TIRS		Results not stable, lower accuracy, TIRS band 11 not stable	
Other	Day and night	Accurate in MODIS	Limitations, low applicability	TERRA/MODIS TERRA/ASTER VIIRS
	Separate temperature	Accurate in ASTER	Not stable, limitations, low applicability	
	Gray matters	Good for grey matters	Sensitive in noise	

4.2. Comparing the Difference between Core Urban and Non-Urban Area

Many studies have documented the use of LST data to observe meso-scale temperature differences between urban and rural areas in cities worldwide [156,208,209]. The land surface temperature (LST) of core urban areas is generally higher than the surrounding rural areas, and has a strong correlation with land cover [153]. UHII analysis is the most common method to compute the magnitude and extent of UHI by evaluating the LST difference between urban and surrounding non-urban areas [162]. These analyses are often supported with auxiliary land surface information, such as land cover and impervious surface area (ISA). Deterministic models generally are generally based on more complex models that compute the intensity of UHIRIP in space and time. Remotely sensed data are used at different modeling levels, either as the input parameters to characterize the different surface covers, or in assimilation procedures, which aim to retrieve adequate parameters for the LST computation. Some examples of these studies are shown in Table 5. UHI intensity was typically quantified in two steps in these studies [60]. First, urban and non-urban areas were defined and delineated from land cover or ISA maps. Urban areas are usually defined as land with a relatively higher proportion of ISA [38,95], whereas non-urban areas have various definitions in different studies, but generally include non-urban land cover classes. Different sized rural and suburban zones have been used as reference areas. Other land covers, such as water bodies, cropland, forest, and low-intensity ISA, have also been used as references in the studies [101]. Second, the area-weighted mean urban-reference LST differences were calculated to reflect the UHI intensity [69,210] or magnitude. Some studies identified "hotspots" based on positive UHI intensity in certain time periods [211,212]. A positive value of UHI intensity indicated an urban heating effect, while a negative value represented a cooling effect. A few studies also quantified the UHI intensity using small numbers of representative pixels in urban and reference areas instead of the area-weighted mean value for the purpose of surface-air UHI comparison [122–124] or UHI attribution analysis [125,126]. The urban-reference difference method facilitates a comparative analysis of UHIs among cities and urban agglomerations, regions, and across the globe, but the validity of such comparisons can be limited by the large uncertainties associated with urban and reference definitions [68]. Recent research [97] performed a comprehensive and consistent analysis of surface UHI and UHIRIP using Landsat LST

ARD time series and dynamic land cover datasets in the Sioux Falls, SD, area. It shows that the use of time series of LST and land change dynamic data provided a consistent and quantitative analysis for the distribution and change of UHI intensity and UHIRIP (Figure 4). We further discuss limitations in Section 5.

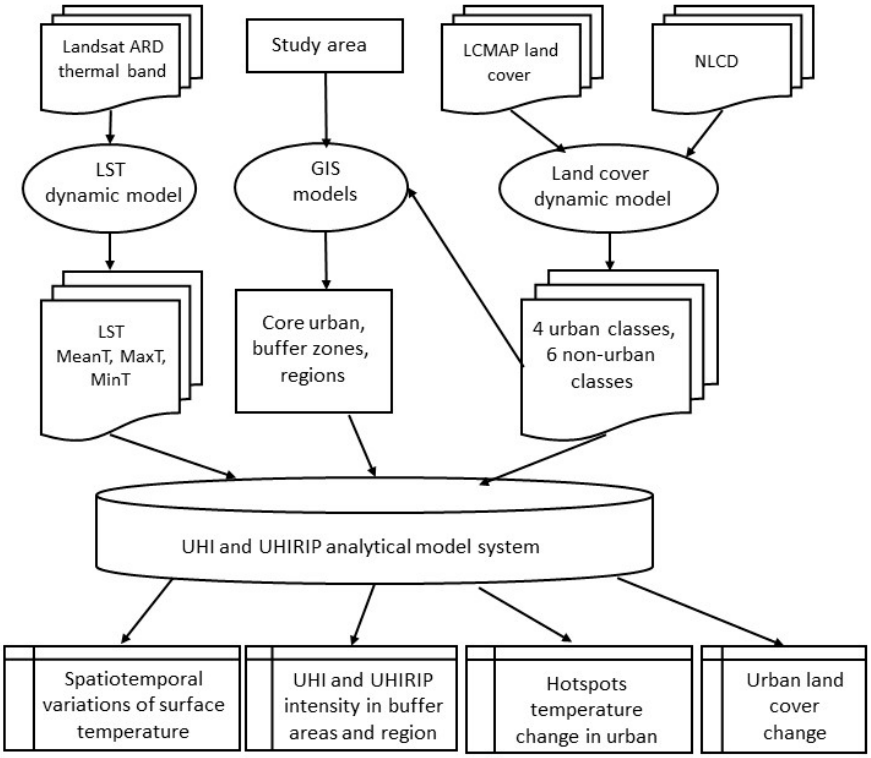

Figure 4. A general workflow chart of the use of time series of LST and land change dynamic data that provides a consistent and quantitative analysis for the distribution and change of UHI intensity and UHIRIP in Sioux Falls, SD.

4.3. UHI and UHIRIP Analysis by Using Urban Ecological Indices

Many studies have compared UHIRIP to ecological indices [103,149,213–215], vegetation fraction, and percent ISA, finding strong correlations with mean LST. Landscape metrics indicate that urban landscape configuration also influences the surface UHIRIP [216]. The latest vegetation index methods and inference methods use remote sensing to compute a reduction factor (such as Kc or Priestley Taylor-alpha parameters) for the estimation of the actual UHI [203]. Different papers deal with these approaches in the various journals, and these approaches use land cover [217,218], LST pattern [219,220], and a combination of land cover and LST pattern [221–223] as monitoring indicators of UHI.

Urban ecological status is closely related to the quality of human life and the development of urban economies. A timely and objective understanding of urban ecological status, particularly in urban and non-urban interface areas [224], has become an increasing important. Scientists have been developing a remote sensing-based ecological index for the measure of urban ecological status under UHI [213,225]. This urban ecological status index (UESI) aims to integrate four important ecological indicators that are frequently used in evaluating urban ecology. The four indicators include greenness, wetness, dryness, and heat, and can be represented by four remote sensing indices or components: NDVI, normalized difference built-up and soil index (NDBSI), wetness component of the tasseled cap transformation (Wet), and LST, respectively. Instead of a simple or weighted addition of the four indicators, a principal component analysis (PCA) can be utilized to compress the four indicators into one index in order to assess the overall urban ecological status under UHI. The calculation of the UESI can be fully automated, avoiding the need to assign

threshold values or weights during the computing procedure. Therefore, the UESI can be used to easily and objectively assess urban ecological status. Combined with change detection, UESI can also be used to monitor the change of the ecological status of the core urban and surrounding non-urban areas between different years. In practice, the index was successfully applied in a multitemporal ecological status assessment [34]. Pan [221] used the G index spatial aggregation analysis to calculate the urban heat island ratio index, and the landscape metrics to quantify the changes of the spatial pattern of the UHI from the aspects of quantity, shape, and structure. Pan found that the heat island strength had a negative linear correlation with urban vegetation coverage, and a positive logarithmic correlation with urban impervious surface coverage. Bala et al. [226] developed the Urban Heat Intensity Ratio Index (UHIRI) to quantify urban heat intensity. This work analyzed the variation in LST with land cover changes in Varanasi, India, from 1989 to 2018, using Landsat images, and concluded that the replacement of vegetation with urban land cover has a severe impact on increasing UHI intensity.

4.4. Various Statistical Models

Statistical models and machine learning have also been proposed to measure UHI [227]. Among these studies, a Gaussian surface model has been utilized the most because it can provide not only the intensity, but also the spatial extent and the central location of the UHI. The kernel convolution method has also been proposed to study UHI effects because of its high efficiency in characterizing the temperature values over space in a continuous surface [227]. Chun and Guldmann [77] explored the urban determinants of UHI using two-dimensional (2D) and three-dimensional (3D) urban information as the input for spatial statistical models. The results show that solar radiations, open spaces, vegetation, building roof-top areas, and water strongly impact surface temperatures, and that spatial regressions are necessary in order to capture the neighboring effects. Recently, Li et al. [81] estimated UHI intensity by linear regression functions between LST and regionalized ISA. These statistical models could avoid the bias caused by the definitions of urban−rural areas or the choice of the representative pixels, and thus facilitate the comparison of UHI among cities. Szymanowski and Kryza [228] addressed the issue of the potential usefulness of remotely sensed data and their derivatives for UHI modeling. Statistically significant models explained 71% to 85% of the air temperature variance. It has been stressed that remotely sensed data are important sources to model urban air temperature heat islands. However, in all of these studies, such models worked less effectively in cities frequently covered by clouds, in arid landscapes, and in urban agglomerations, so they have only been applied in a few UHI studies to date. Recently, Lai et al. [79] published the statistical estimation of next-day nighttime surface urban heat islands of selected cities. Most previous studies modelled the SUHI variations for the past period, but rarely investigated the estimation for future UHIs, especially at the daily (i.e., day-to-day) scale. To address this issue, this study incorporated both meteorological and surface controls to estimate next-day nighttime UHIs using a support vector machine regression (SVR) model. Some uncertainties exist in terms of the Gaussian modelling and UHI estimators, which may limit estimation accuracy. Nevertheless, by providing a feasible yet simple approach for estimating next-day nighttime UHIs, this study fills a knowledge gap in the UHI estimation and is helpful for supporting adaptation to and mitigation of UHI and UHIRIP.

4.5. Spatial−Temporal Time-Series Algorithm

Advances in computing technology have fostered the development of new and powerful data fusion, gap filling, machine learning, and deep learning techniques that have demonstrated promising results in a wide range of applications [229]. Models to fuse data from multiple sensors and fill gaps can improve UHI monitoring using an ensemble of dense time series of thermal data with a high spatial resolution [199,230]. Zhou et al. [200] presented a new algorithm that focuses on data gap filling using clear observations from

orbit overlap regions to obtain Landsat LST data. Multiple linear regression models were established for each pixel time series to estimate the stable predictions and uncertainties. Liu et al. [83] comprehensively quantified the spatial–temporal patterns of surface urban heat island by investigating the relationship between LST and the land cover types, and the associated landscape components. Such approaches have been used to generate temporally dense and high-resolution LST over long time periods by integrating the observations of Landsat, MODIS, AVHRR, VIIRS, and ECOSTRESS [191,231]. These datasets facilitate subtle analyses of monthly, seasonal, and yearly trends in UHI intensity at regional levels. Machine learning (ML) has become popular in UHI and UHIRIP, but its use has remained restricted to predicting, rather than understanding, the natural world. ML techniques may not be the solution to all the problems remotely sensed data might have. However, these techniques provide a powerful set of tools that deserve serious attention to deal with some relevant UHI and UHIRIP remotely sensed data problems [232]. Lucas [233] points out that ML differs from the broader field of statistics in two respects: (1) the estimation of parameters that relate to the real world is less emphasized, and (2) the driver of the predictions is expected to be the data rather than expert opinion and careful selection of plausible mechanistic models. The Google Earth engine (GEE) is a cloud-based platform for planetary-scale geospatial analysis that brings Google's massive computational capabilities to bear on a variety of high-impact societal and environmental issues [234]. GEE has many functions that could be used to analyze UHI and UHIRIP at local, regional, and global levels (Figure 5). Some research has generated consistent large-scale UHI and UHIRIP analysis based on optimal data and ML algorithm selection using GEE [235,236]. The advanced GEE cloud-based platform and the large number of geosciences and remote sensing datasets archived in GEE were used to analyze land the cover dynamics (236), and the results showed the advantages of using GEE to analyze the spatiotemporal dynamics of the LULCC, vegetation cover, LST, and climate for a long time series, and highlighted the importance of environmental protection. The power here lies in the way a scientist defines their questions and uses machine learning alongside other methods. Techniques for data analysis and interpretation that fully incorporate the temporal dimension remain an area of intense research and represent an important challenge for operational UHI and UHIRIP monitoring.

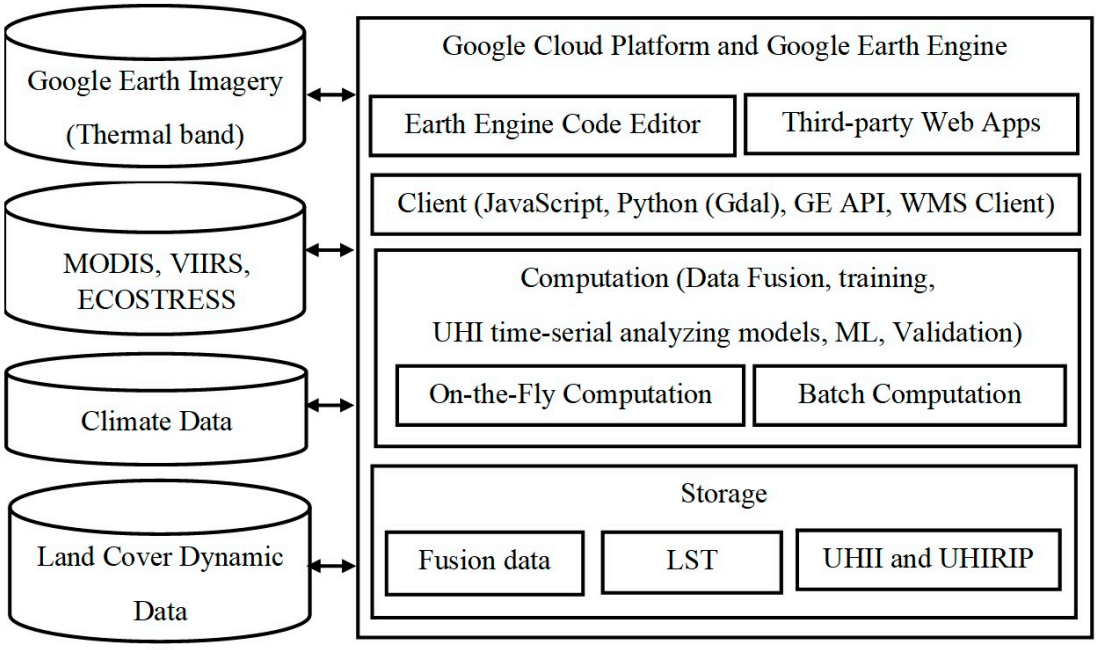

Figure 5. Simplified system diagram using the Google Cloud platform and Google Earth engine for monitoring UHI and UHIRIP.

5. Summary of UHI and UHIRIP Based on Remotely Sensed Data

This review provides an overview of research on UHI and UHIRIP based on remote sensing techniques, sensors, and algorithms, as listed in Tables 3–6, respectively. Much work has been completed on UHIRIP in the last four decades, and we have endeavored to keep updated with new methods and results. A significant research limitation still exists: the quantification of UHI and its regional impacts using high-resolution time-series remotely sensed thermal data in the urban and non-urban interface. Some of the algorithms listed in Table 5 may be the most practical approaches to assess UHI in core urban areas of cities and surrounding areas, but characterization of UHI across broad areas is necessary in order to inform monitoring, reporting, science, and policy. Being able to relate LST to UHI is especially important when such datasets are being used to inform policy decisions or to communicate outside of the scientific community. The increasing availability of remotely sensed data across a range of spatial resolutions and temporal frequencies, and technological improvements in image processing capacity and storage, have led to advances in the methods used to monitor UHI more frequently and accurately.

Assessing the uncertainty and accuracy of UHI data is important. A sensitivity analysis not only provides a framework for assessing the potential for bias and the extent of uncertainty in UHI estimates, but also reveals significant factors that determine the extent of UHIRIP in the urban and non-urban interface. Oleson et al. [237] developed an approach to evaluate the robustness of models used to simulate urban heat islands in different environments. The findings indicated that heat storage and sensible heat flux are most sensitive to uncertainties in the input parameters within the atmospheric and surface conditions considered. Sensitivity studies indicate that it is important to not only to accurately characterizing the structure of the urban area, but also to ensuring that the input data reflect the thermal admittance properties of each of the city surfaces.

Currently, a wide variety of methods are employed to characterize UHI for major cities worldwide (Table 5), although most of the applications cited were limited to small areas because of data availability and constraints of storage and computing resources. With the development of gap filling and data fusion models [238], advances in high-performance computing (HPC), and cheaper storage, applications based on high-resolution time series at larger or even regional scales will become the mainstream in the near future [199,231]. While much of the methodological variation described here will persist, future methods will evolve and adapt to greater data volumes and processing capabilities [239]. Legacy change mapping methods that rely on analyst interactions with individual scenes should decline over time given the improved ability to process and characterize time series of rich high-resolution thermal data. However, such spatial−temporal methods that are based on gap filling and data fusion should match the institutional requirements for accuracy. Near-term research objectives will require robust validation datasets in establishing which data-intensive methods are the most appropriate for quantifying UHI over large areas. Techniques for LST data analysis and interpretation that fully incorporate the temporal dimension still require intense research and represent an important challenge for operational UHI research in order to meet management needs.

Technological advances that include machining leaning and artificial intelligence in UHI and UHIRIP using remotely sensed data have led to an explosion of UHI and UHIRIP profiling data from large numbers of multiple data sources [233,240]. This rapid increase in the remotely sensed data dimension and acquisition rate is challenging conventional analysis strategies. Modern machine learning methods, such as deep learning, promise to leverage very large datasets for finding a hidden structure within them, and for making accurate predictions [232]. Deep learning methods are a powerful complement to classical machine learning tools and other analysis strategies, and have been used in a number of applications in UHII and remotely sensed image analyses [241]. The explainable artificial intelligence in UHII and UHIRIP modeling has become more and more important [242]. Interpretable machine learning methods either target a direct understanding of the model

architecture (i.e., model-based interpretability) or interpret the model by analyzing the model behavior (post hoc interpretability) [242].

Currently, most of the time-series algorithms used to map UHIRIP include data from the temporal domain of AVHRR and MODIS, and the spatial domain of the data is almost entirely neglected. Although these datasets with a lower spatial resolution and higher temporal frequency can detect a change of UHI in real time, they often lack pertinent spatial detail. Even though many UHI analysis algorithms have been developed [60], most of the UHI monitoring data derived from the Landsat archive are provided in a time frame that is not near enough to real time to be relevant for specific management needs. With the advances in HPC and cheaper storage, applications based on Landsat time series at continental or even global scales will be the mainstream in the next few years.

To date, information from Landsat time-series thermal data has taken the form of statistical metrics, change metrics, pattern distribution, or trend components used in UHI impact applications [243]. Improvement of existing approaches, as well as the inclusion of novel techniques, often imported and adapted from other disciplines, are important to fully capitalize on the thermal data in order to produce monthly, seasonal, and annual LST results that meet a wide range of UHI and UHIRIP research needs. Landsat-9, which will be launched in September 2021, will continue collecting images of the Earth's surface in visible, near-infrared, and shortwave-infrared bands, as well as the thermal infrared radiation, or heat, of the Earth's surface from two thermal bands. The future European Space Agency's LSTM (Land Surface Temperature Monitoring) or Sentinel 8 mission will carry a high spatial−temporal resolution thermal infrared sensor to provide records of land-surface temperature. Land-surface temperature measurements are key variables to understand and respond to climate variability and natural hazards, such as urban heat island issues. The main objective of LSTM is to deliver global high spatial−temporal day- and night-time land surface temperature measurements. LSTM will operate from a low-Earth, polar orbit, to map both land-surface temperature and rates of evapotranspiration. It will be able to identify the temperatures of individual fields and image the Earth every three days at a 50 m resolution. Another future thermal sensor is Thermal infraRed Imaging Satellite for High-resolution Natural resource Assessment (TRISHNA), which is a future high-resolution space-time mission in the thermal infrared (TIR) led jointly by the French (CNES) and Indian (ISRO) space agencies. One of scientific objectives guiding the definition of the mission is the monitoring of the urban environment. TRISHNA will be positioned on a polar orbit and provide a revisit of three passages over 8 days with global coverage. The time of passage around 13:00 p.m. LST allows thermal data to be collected in the middle of the day, but also in the middle of the night. The instrument will offer four thermal channels (8.6 µm, 9.1 µm, 10.4 µm, and 11.6 µm) and six optical channels (485 nm, 555 nm, 650 nm, 860 nm, 1380 nm, and 1650 nm) with a spatial resolution between 50 m and 60 m for all channels. All of these observations acquired from thermal remote sensing will provide more valuable information for natural resource management, hazard monitoring, and scientific research and applications.

6. Future Research Directions

Remote sensing technology has been widely applied in the research of UHI and UHIRIP. The most important advantage of using remote sensing thermal data is the wall-to-wall coverage of UHI patterns that can meet the needs of spatial and temporal analyses. Remotely sensed data can be used to investigate the surface temperatures of cities and urban agglomerations for various ecosystems with different climate conditions, for example tropical and sub-tropical, temperate and cold temperate, coastal and inland, and arid and semi-arid land at regional scales. These studies are needed to describe surface temperature characteristics in these specific environments and how climate change may be modulating UHI patterns. UHIRIP produces an aggregate impact on weather conditions, land use, human health, biodiversity, ecosystem security, economics, and urban planning [16,244].

Land surface temperature and emissivity retrieval (separation) has always been challenging. Generally, the LSE values needed to apply the method have been estimated from a procedure that uses the visible and near-infrared bands. The algorithm was created using the brightness temperature of the thermal and emissivity of different land cover types, derived from visible and near-infrared bands of various sensors. Compared with field-based observation, remote sensing offers the advantages of a harmonized, long-term, and spatially extensive record to observe LST change. The retrieved LSTs are verified using the near surface temperature of weather station datasets, which will help to improve the accuracy of LST derived from thermal bands. The difference between retrieved LST and Automatic Weather Station (AWS) data indicates that the technique works by giving an error of ± 3 °C [245]. These differences can be because of the difference between the resolutions of thermal and visible bands, and a comparison was made between the point measurement (AWS data) 2 m above the surface and surface temperature (retrieved LST). Communicating the results of time-series LST studies that are based on both field weather station observations and remote-sensing time-series data to urban planners, policymakers, and the general public could help inform urban design and decision making.

Using temporally dense time series of remotely sensed data at a high spatial resolution is a growing trend in UHI and UHIRIP research, facilitated by increasing computer capabilities to handle big datasets, machine leaning, deep learning, and Google Earth Engine applications. Landsat ARD, in particular, has great potential to derive LST. Models used to fuse data from across multiple sensors will be developed to increase data temporal density and spatial resolution. Moreover, future sensor improvement on Landsat and aircraft thermal data are possible options. On the other hand, in order to determine the temporal variation of LST using satellite data with restricted overpass times, it appears necessary to use long-time weather station observations to investigate diurnal UHI in various ecosystems, although some new sensors (e.g., ECOSTRESS) can provide this information. Future research is anticipated to improve on methods to simultaneously derive LST and land surface emission (LSE) from hyperspectral TIR, multi spectral-temporal, and TIR-microwave data; additionally, future methods will consider aerosol and cirrus effects [18]. Another viable angle of potential future studies is urban development strategies for mitigating UHI, such as increasing vegetation and water surfaces in urban development.

Climate models are the only tools that account for the complex set of processes that will determine future climate change at both a global and regional level, and assessing regional impacts of climate change begins with the development of climate projections at relevant temporal and spatial scales [246]. The most current existing climate change modeling covers large geographic areas at regional and global levels with relatively low spatial resolutions (>10 km). In the future, LST that is derived from remotely sensed data will support climate change modeling (regional climate models and statistical downscaling models) in UHI and UHIRIP analyses in urban and surrounding areas.

Our analysis indicated that determination is still a central topic of UHI research. Modeling will continue to provide vital and useful results on the spatiotemporal assessment of UHI, especially when models more effectively combine thermal data from multiple sensors. ML (DL) and AI are continuing to grow in popularity in UHI and UHIRIP research. For time series analyses with remote sensing data, a cloud computing platform such as GEE could bring about a substantial change in UHI and UHIRIP analyses, as they have the capability to process big remote sensing datasets and assess the spatiotemporal dynamics of the area quickly. A better integration of remote sensing and station measurements into models is expected. This study also suggests that direct and indirect UHIRIP, especially human health issues, heat wave impacts, air pollution, and ecological security, will receive increasing scientific attention in the future. Research on controlling and adapting to UHI impacts may warrant special attention. The interaction of UHI and UHIRIP, and their changes to LULC based on urban planning, are actively being studied.

Author Contributions: Original draft preparation, H.S.; review and editing with ideas and inputs, G.X., R.A., K.G. and Q.Z. All authors have read and agreed to the published version of the manuscript.

Funding: This research received no external funding.

Institutional Review Board Statement: Not applicable.

Informed Consent Statement: Not applicable.

Data Availability Statement: Not applicable.

Acknowledgments: We are grateful to the USGS National Land Imaging Program for supporting this research. We would like to thank Carol Deering for assistance in collecting and preparing the literary material. This manuscript was improved thanks to comments and suggestions from Norman Bliss, Matthew Rigge, and Thomas Adamson. Hua Shi and Qiang Zhou's work was performed under USGS contracts G13PC00028 and 140G0119C0001. For Kevin Gallo, the scientific results and conclusions, as well as any views or opinions expressed herein, are those of the author and do not necessarily reflect those of NOAA or the Department of Commerce. Any use of trade, firm, or product names is for descriptive purposes only and does not imply endorsement by the U.S. Government.

Conflicts of Interest: The authors declare no conflict of interest. The funding sponsors had no role in the design of the study; in the collection, analyses, or interpretation of data; in the writing of the manuscript; and in the decision to publish the results.

References

1. Radeloff, V.C.; Hammer, R.B.; Stewart, S.I.; Fried, J.S.; Holcomb, S.S.; McKeefry, J.F. The Wildland–Urban Interface in the United States. *Ecol. Appl.* **2005**, *15*, 799–805. [CrossRef]
2. Shi, H.; Singh, A.; Kant, S.; Zhu, Z.; Waller, E. Integrating habitat status, human population pressure, and protection status into biodiversity conservation priority setting. *Conserv. Biol.* **2005**, *19*, 1273–1285. [CrossRef]
3. Seto, K.C.; Shepherd, J.M. Global urban land-use trends and climate impacts. *Curr. Opin. Environ. Sustain.* **2009**, *1*, 89–95. [CrossRef]
4. Ager, A.A.; Vaillant, N.M.; Finney, M.A. A comparison of landscape fuel treatment strategies to mitigate wildland fire risk in the urban interface and preserve old forest structure. *For. Ecol. Manag.* **2010**, *259*, 1556–1570. [CrossRef]
5. Chang, Q.; Liu, X.; Wu, J.; He, P. MSPA-based urban green infrastructure planning and management approach for urban sustainability: Case study of longgang in China. *J. Urban Plan. Dev.* **2015**, *141*. [CrossRef]
6. Voogt, J.A.; Oke, T.R. Thermal remote sensing of urban climates. *Remote Sens. Environ.* **2003**, *86*, 370–384. [CrossRef]
7. Weng, Q. Thermal infrared remote sensing for urban climate and environmental studies: Methods, applications, and trends. *ISPRS J. Photogramm. Remote Sens.* **2009**, *64*, 335–344. [CrossRef]
8. Massad, R.S.; Lathière, J.; Strada, S.; Perrin, M.; Personne, E.; Stéfanon, M.; Stella, P.; Szopa, S.; de Noblet-Ducoudré, N. Reviews and syntheses: Influences of landscape structure and land uses on local to regional climate and air quality. *Biogeosciences* **2019**, *16*, 2369–2408. [CrossRef]
9. Raalte, L.V.; Nolan, M.; Thakur, P.; Xue, S.; Parker, N. *Economic Assessment of the Urban Heat Island Effect*; 60267369; AECOM Australia Pty Ltd.: Melbourne, Australia, 2012. Available online: https://www.melbourne.vic.gov.au/SiteCollectionDocuments/eco-assessment-of-urban-heat-island-effect.pdf (accessed on 20 May 2020).
10. Oke, T.R. The energetic basis of the urban heat island. *Q. J. R. Meteorol. Soc.* **1982**, *108*, 1–24. [CrossRef]
11. Hall, F.G.; Huemmrich, K.F.; Goetz, S.J.; Sellers, P.J.; Nickeson, J.E. Satellite remote sensing of surface energy balance: Success, failures, and unresolved issues in FIFE. *J. Geophys. Res.* **1992**, *97*, 19061–19089. [CrossRef]
12. Velasco, E. Go to field, look around, measure and then run models. *Urban Clim.* **2018**, *24*, 231–236. [CrossRef]
13. Gallo, K.P.; Tarpley, J.D.; McNab, A.L.; Karl, T.R. Assessment of urban heat islands: A satellite perspective. *Atmos. Res.* **1995**, *37*, 37–43. [CrossRef]
14. Courault, D.; Seguin, B.; Olioso, A. Review on estimation of evapotranspiration from remote sensing data: From empirical to numerical modeling approaches. *Irrig. Drain. Syst.* **2005**, *19*, 223–249. [CrossRef]
15. Dorigo, W.A.; Zurita-Milla, R.; de Wit, A.J.W.; Brazile, J.; Singh, R.; Schaepman, M.E. A review on reflective remote sensing and data assimilation techniques for enhanced agroecosystem modeling. *Int. J. Appl. Earth Obs. Geoinf.* **2007**, *9*, 165–193. [CrossRef]
16. Rasul, A.; Balzter, H.; Smith, C.; Remedios, J.; Adamu, B.; Sobrino, J.; Srivanit, M.; Weng, Q. A Review on Remote Sensing of Urban Heat and Cool Islands. *Land* **2017**, *6*, 38. [CrossRef]
17. Weng, Q.; Fu, P. Modeling diurnal land temperature cycles over Los Angeles using downscaled GOES imagery. *ISPRS J. Photogramm. Remote Sens.* **2014**, *97*, 78–88. [CrossRef]
18. Weng, Q.; Firozjaei, M.K.; Sedighi, A.; Kiavarz, M.; Alavipanah, S.K. Statistical analysis of surface urban heat island intensity variations: A case study of Babol city, Iran. *GIScience Remote Sens.* **2019**, *56*, 576–604. [CrossRef]
19. Ward, K.; Lauf, S.; Kleinschmit, B.; Endlicher, W. Heat waves and urban heat islands in Europe: A review of relevant drivers. *Sci. Total Environ.* **2016**, *569–570*, 527–539. [CrossRef] [PubMed]

20. Zhu, Z. Change detection using landsat time series: A review of frequencies, preprocessing, algorithms, and applications. *ISPRS J. Photogramm. Remote Sens.* **2017**, *130*, 370–384. [CrossRef]
21. Du, W.; Qin, Z.; Fan, J.; Gao, M.; Wang, F.; Abbasi, B. An efficient approach to remove thick cloud in VNIR bands of multi-temporal remote sensing images. *Remote Sens.* **2019**, *11*, 1284. [CrossRef]
22. Ling, F.; Zhang, T. A numerical model for surface energy balance and thermal regime of the active layer and permafrost containing unfrozen water. *Cold Reg. Sci. Technol.* **2004**, *38*, 1–15. [CrossRef]
23. Atkinson, B.W. Numerical modelling of urban heat-island intensity. *Bound.-Layer Meteorol.* **2003**, *109*, 285–310. [CrossRef]
24. Oke, T.R. The distinction between canopy and boundary-layer urban heat Islands. *Atmosphere* **1976**, *14*, 268–277. [CrossRef]
25. Kim, H.H. Urban heat island. *Int. J. Remote Sens.* **1992**, *13*, 2319–2336. [CrossRef]
26. Taha, H. Urban climates and heat islands: Albedo, evapotranspiration, and anthropogenic heat. *Energy Build.* **1997**, *25*, 99–103. [CrossRef]
27. Oke, T.R. *The Heat Island of the Urban Boundary Layer: Characteristics, Causes and Effects*; Springer: Dordrecht, The Netherlands, 1995; Volume 277. [CrossRef]
28. Stone, B., Jr.; Rodgers, M.O. Urban form and thermal efficiency: How the design of cities influences the urban heat island effect. *J. Am. Plan. Assoc.* **2001**, *67*, 186–198. [CrossRef]
29. Hansen, J.; Ruedy, R.; Sato, M.; Imhoff, M.; Lawrence, W.; Easterling, D.; Peterson, T.; Karl, T. A closer look at United States and global surface temperature change. *J. Geophys. Res. Atmos.* **2001**, *106*, 23947–23963. [CrossRef]
30. Golden, J.S. The Built Environment Induced Urban Heat Island Effect in Rapidly Urbanizing Arid Regions—A Sustainable Urban Engineering Complexity. *Environ. Sci.* **2004**, *1*, 321–349. [CrossRef]
31. Bowler, D.E.; Buyung-Ali, L.; Knight, T.M.; Pullin, A.S. Urban greening to cool towns and cities: A systematic review of the empirical evidence. *Landsc. Urban Plan.* **2010**, *97*, 147–155. [CrossRef]
32. Chow, W.T.L.; Brennan, D.; Brazel, A.J. Urban Heat Island Research in Phoenix, Arizona: Theoretical Contributions and Policy Applications. *Bull. Am. Meteorol. Soc.* **2011**, *93*, 517–530. [CrossRef]
33. Qin, Y. A review on the development of cool pavements to mitigate urban heat island effect. *Renew. Sustain. Energy Rev.* **2015**, *52*, 445–459. [CrossRef]
34. Xu, H.Q. A remote sensing urban ecological index and its application. *Shengtai Xuebao Acta Ecol. Sin.* **2013**, *33*, 7853–7862. [CrossRef]
35. Memon, R.A.; Leung, D.Y.C.; Liu, C.-H. An investigation of urban heat island intensity (UHII) as an indicator of urban heating. *Atmos. Res.* **2009**, *94*, 491–500. [CrossRef]
36. Sinha, P.; Coville, R.C.; Hirabayashi, S.; Lim, B.; Endreny, T.A.; Nowak, D.J. Modeling lives saved from extreme heat by urban tree cover☆. *Ecol. Model.* **2021**, *449*, 109553. [CrossRef]
37. Li, K.; Yu, Z. Comparative and combinative study of urban heat island in Wuhan City with remote sensing and CFD simulation. *Sensors* **2008**, *8*, 6692–6703. [CrossRef]
38. Chen, X.L.; Zhao, H.M.; Li, P.X.; Yin, Z.Y. Remote sensing image-based analysis of the relationship between urban heat island and land use/cover changes. *Remote Sens. Environ.* **2006**, *104*, 133–146. [CrossRef]
39. Streutker, D.R. A remote sensing study of the urban heat island of Houston, Texas. *Int. J. Remote Sens.* **2002**, *23*, 2595–2608. [CrossRef]
40. Lee, H.Y. An application of NOAA AVHRR thermal data to the study of urban heat islands. *Atmos. Environ. Part B Urban Atmos.* **1993**, *27*, 1–13. [CrossRef]
41. Gallo, K.P.; McNab, A.L.; Karl, T.R.; Brown, J.F.; Hood, J.J.; Tarpley, J.D. The use of NOAA AVHRR data for assessment of the urban heat island effect. *J. Appl. Meteorol.* **1993**, *32*, 899–908. [CrossRef]
42. Kotharkar, R.; Ramesh, A.; Bagade, A. Urban Heat Island studies in South Asia: A critical review. *Urban Clim.* **2018**, *24*, 1011–1026. [CrossRef]
43. Bullock, E.L.; Woodcock, C.E.; Holden, C.E. Improved change monitoring using an ensemble of time series algorithms. *Remote Sens. Environ.* **2019**. [CrossRef]
44. Cohen, W.B.; Yang, Z.; Healey, S.P.; Kennedy, R.E.; Gorelick, N. A LandTrendr multispectral ensemble for forest disturbance detection. *Remote Sens. Environ.* **2018**, *205*, 131–140. [CrossRef]
45. Liu, C.; Zhang, Q.; Luo, H.; Qi, S.; Tao, S.; Xu, H.; Yao, Y. An efficient approach to capture continuous impervious surface dynamics using spatial-temporal rules and dense Landsat time series stacks. *Remote Sens. Environ.* **2019**, *229*, 114–132. [CrossRef]
46. Shi, H.; Rigge, M.; Homer, C.G.; Xian, G.; Meyer, D.K.; Bunde, B. Historical Cover Trends in a Sagebrush Steppe Ecosystem from 1985 to 2013: Links with Climate, Disturbance, and Management. *Ecosystems* **2018**, *21*, 913–929. [CrossRef]
47. Zhu, Z.; Gallant, A.L.; Woodcock, C.E.; Pengra, B.; Olofsson, P.; Loveland, T.R.; Jin, S.; Dahal, D.; Yang, L.; Auch, R.F. Optimizing selection of training and auxiliary data for operational land cover classification for the LCMAP initiative. *ISPRS J. Photogramm. Remote Sens.* **2016**, *122*, 206–221. [CrossRef]
48. Dwyer, J.L.; Roy, D.P.; Sauer, B.; Jenkerson, C.B.; Zhang, H.K.; Lymburner, L. Analysis ready data: Enabling analysis of the landsat archive. *Remote Sens.* **2018**, *10*, 1363. [CrossRef]
49. Weng, Q.; Larson, R.C. Satellite Remote Sensing of Urban Heat Islands: Current Practice and Prospects. In *Geo-Spatial Technologies in Urban Environments*; 2005; pp. 91–111. Available online: https://link.springer.com/chapter/10.1007%2F3-540-26676-3_10 (accessed on 2 February 2020). [CrossRef]

50. Jiang, G.M.; Li, Z.L.; Nerry, F. Land surface emissivity retrieval from combined mid-infrared and thermal infrared data of MSG-SEVIRI. *Remote Sens. Environ.* **2006**, *105*, 326–340. [CrossRef]
51. Kalma, J.D.; McVicar, T.R.; McCabe, M.F. Estimating land surface evaporation: A review of methods using remotely sensed surface temperature data. *Surv. Geophys.* **2008**, *29*, 421–469. [CrossRef]
52. Racoviteanu, A.E.; Williams, M.W.; Barry, R.G. Optical remote sensing of glacier characteristics: A review with focus on the Himalaya. *Sensors* **2008**, *8*, 3355–3383. [CrossRef]
53. Rizwan, A.M.; Dennis, L.Y.C.; Liu, C. A review on the generation, determination and mitigation of Urban Heat Island. *J. Environ. Sci.* **2008**, *20*, 120–128. [CrossRef]
54. Sailor, D.J. A review of methods for estimating anthropogenic heat and moisture emissions in the urban environment. *Int. J. Climatol.* **2011**, *31*, 189–199. [CrossRef]
55. Li, Z.L.; Tang, B.H.; Wu, H.; Ren, H.; Yan, G.; Wan, Z.; Trigo, I.F.; Sobrino, J.A. Satellite-derived land surface temperature: Current status and perspectives. *Remote Sens. Environ.* **2013**, *131*, 14–37. [CrossRef]
56. Ngie, A.; Abutaleb, K.; Ahmed, F.; Darwish, A.; Ahmed, M. Assessment of urban heat island using satellite remotely sensed imagery: A review. *S. Afr. Geogr. J.* **2014**, *96*, 198–214. [CrossRef]
57. Huang, Q.; Lu, Y. Urban heat island research from 1991 to 2015: A bibliometric analysis. *Theor. Appl. Climatol.* **2018**, *131*, 1055–1067. [CrossRef]
58. Zhang, Y.; Thenkabail, P.S.; Wang, P. A bibliometric profile of the Remote Sensing Open Access Journal published by MDPI between 2009 and 2018. *Remote Sens.* **2019**, *11*, 91. [CrossRef]
59. Deilami, K.; Kamruzzaman, M.; Liu, Y. Urban heat island effect: A systematic review of spatio-temporal factors, data, methods, and mitigation measures. *Int. J. Appl. Earth Obs. Geoinf.* **2018**, *67*, 30–42. [CrossRef]
60. Zhou, D.; Xiao, J.; Bonafoni, S.; Berger, C.; Deilami, K.; Zhou, Y.; Frolking, S.; Yao, R.; Qiao, Z.; Sobrino, J.A. Satellite remote sensing of surface urban heat islands: Progress, challenges, and perspectives. *Remote Sens.* **2019**, *11*, 48. [CrossRef]
61. Becker, F.; Li, Z.L. Surface temperature and emissivity at various scales: Definition, measurement and related problems. *Remote Sens. Rev.* **1995**, *12*, 225–253. [CrossRef]
62. Dash, P.; Göttsche, F.M.; Olesen, F.S.; Fischer, H. Land surface temperature and emissivity estimation from passive sensor data: Theory and practice-current trends. *Int. J. Remote Sens.* **2002**, *23*, 2563–2594. [CrossRef]
63. Miles, V.; Esau, I. Seasonal and spatial characteristics of Urban Heat Islands (UHIs) in northern West Siberian cities. *Remote Sens.* **2017**, *9*, 989. [CrossRef]
64. Trlica, A.; Hutyra, L.R.; Schaaf, C.L.; Erb, A.; Wang, J.A. Albedo, Land Cover, and Daytime Surface Temperature Variation Across an Urbanized Landscape. *Earths Future* **2017**, *5*, 1084–1101. [CrossRef]
65. Bonafoni, S. Spectral index utility for summer urban heating analysis. *J. Appl. Remote Sens.* **2015**, *9*. [CrossRef]
66. Wong, M.S.; Nichol, J.E. Spatial variability of frontal area index and its relationship with urban heat island intensity. *Int. J. Remote Sens.* **2013**, *34*, 885–896. [CrossRef]
67. Jin, M.S. Developing an Index to Measure Urban Heat Island Effect Using Satellite Land Skin Temperature and Land Cover Observations. *J. Clim.* **2012**, *25*, 6193–6201. [CrossRef]
68. Wu, C.D.; Lung, S.C.C.; Jan, J.F. Development of a 3-D urbanization index using digital terrain models for surface urban heat island effects. *Isprs J. Photogramm. Remote Sens.* **2013**, *81*, 1–11. [CrossRef]
69. Hu, L.Q.; Brunsell, N.A. The impact of temporal aggregation of land surface temperature data for surface urban heat island (SUHI) monitoring. *Remote Sens. Environ.* **2013**, *134*, 162–174. [CrossRef]
70. Zhang, Z.W.; Du, Q.Y. A Bayesian Kriging Regression Method to Estimate Air Temperature Using Remote Sensing Data. *Remote Sens.* **2019**, *11*, 767. [CrossRef]
71. Wicki, A.; Parlow, E. Multiple Regression Analysis for Unmixing of Surface Temperature Data in an Urban Environment. *Remote Sens.* **2017**, *9*, 684. [CrossRef]
72. Dai, Z.; Guldmann, J.M.; Hu, Y. Spatial regression models of park and land-use impacts on the urban heat island in central Beijing. *Sci. Total Environ.* **2018**, *626*, 1136–1147. [CrossRef]
73. Song, J.; Du, S.; Feng, X.; Guo, L. The relationships between landscape compositions and land surface temperature: Quantifying their resolution sensitivity with spatial regression models. *Landsc. Urban Plan.* **2014**, *123*, 145–157. [CrossRef]
74. Sellers, P.J.; Meeson, B.W.; Hall, F.G.; Asrar, G.; Murphy, R.E.; Schiffer, R.A.; Bretherton, F.P.; Dickinson, R.E.; Ellingson, R.G.; Field, C.B.; et al. Remote sensing of the land surface for studies of global change: Models—Algorithms—Experiments. *Remote Sens. Environ.* **1995**, *51*, 3–26. [CrossRef]
75. Du, S.H.; Xiong, Z.Q.; Wang, Y.C.; Guo, L. Quantifying the multilevel effects of landscape composition and configuration on land surface temperature. *Remote Sens. Environ.* **2016**, *178*, 84–92. [CrossRef]
76. Shahraiyni, H.T.; Sodoudi, S.; El-Zafarany, A.; Abou El Seoud, T.; Ashraf, H.; Krone, K. A Comprehensive Statistical Study on Daytime Surface Urban Heat Island during Summer in Urban Areas, Case Study: Cairo and Its New Towns. *Remote Sens.* **2016**, *8*, 643. [CrossRef]
77. Chun, B.; Guldmann, J.M. Spatial statistical analysis and simulation of the urban heat island in high-density central cities. *Landsc. Urban Plan.* **2014**, *125*, 76–88. [CrossRef]
78. Ho, H.C.; Knudby, A.; Sirovyak, P.; Xu, Y.M.; Hodul, M.; Henderson, S.B. Mapping maximum urban air temperature on hot summer days. *Remote Sens. Environ.* **2014**, *154*, 38–45. [CrossRef]

79. Lai, J.; Zhan, W.; Quan, J.; Bechtel, B.; Wang, K.; Zhou, J.; Huang, F.; Chakraborty, T.; Liu, Z.; Lee, X. Statistical estimation of next-day nighttime surface urban heat islands. *ISPRS J. Photogramm. Remote Sens.* **2021**, *176*, 182–195. [CrossRef]
80. Huang, X.; Wang, Y. Investigating the effects of 3D urban morphology on the surface urban heat island effect in urban functional zones by using high-resolution remote sensing data: A case study of Wuhan, Central China. *ISPRS J. Photogramm. Remote Sens.* **2019**, *152*, 119–131. [CrossRef]
81. Li, H.; Zhou, Y.; Li, X.; Meng, L.; Wang, X.; Wu, S.; Sodoudi, S. A new method to quantify surface urban heat island intensity. *Sci. Total Environ.* **2018**, *624*, 262–272. [CrossRef] [PubMed]
82. Berger, C.; Rosentreter, J.; Voltersen, M.; Baumgart, C.; Schmullius, C.; Hese, S. Spatio-temporal analysis of the relationship between 2D/3D urban site characteristics and land surface temperature. *Remote Sens. Environ.* **2017**, *193*, 225–243. [CrossRef]
83. Liu, K.; Su, H.B.; Li, X.K.; Wang, W.M.; Yang, L.J.; Liang, H. Quantifying Spatial-Temporal Pattern of Urban Heat Island in Beijing: An Improved Assessment Using Land Surface Temperature (LST) Time Series Observations From LANDSAT, MODIS, and Chinese New Satellite GaoFen-1. *IEEE J. Sel. Top. Appl. Earth Obs. Remote Sens.* **2016**, *9*, 2028–2042. [CrossRef]
84. Fu, P.; Weng, Q.H. Consistent land surface temperature data generation from irregularly spaced Landsat imagery. *Remote Sens. Environ.* **2016**, *184*, 175–187. [CrossRef]
85. Liang, B.Q.; Weng, Q.H. Assessing Urban Environmental Quality Change of Indianapolis, United States, by the Remote Sensing and GIS Integration. *IEEE J. Sel. Top. Appl. Earth Obs. Remote Sens.* **2011**, *4*, 43–55. [CrossRef]
86. Dousset, B.; Gourmelon, F. Satellite multi-sensor data analysis of urban surface temperatures and landcover. *ISPRS J. Photogramm. Remote Sens.* **2003**, *58*, 43–54. [CrossRef]
87. Chakraborty, T.; Lee, X. A simplified urban-extent algorithm to characterize surface urban heat islands on a global scale and examine vegetation control on their spatiotemporal variability. *Int. J. Appl. Earth Obs. Geoinf.* **2019**, *74*, 269–280. [CrossRef]
88. Mpakairia, K.S.; Muvengwi, J. Night-time lights and their influence on summer night land surface temperature in two urban cities of Zimbabwe: A geospatial perspective. *Urban Clim.* **2019**. [CrossRef]
89. Zhang, Y.; Jiang, P.; Zhang, H.; Cheng, P. Study on urban heat island intensity level identification based on an improved restricted Boltzmann machine. *Int. J. Environ. Res. Public Health* **2018**, *15*, 186. [CrossRef]
90. Tran, D.X.; Pla, F.; Latorre-Carmona, P.; Myint, S.W.; Gaetano, M.; Kieu, H.V. Characterizing the relationship between land use land cover change and land surface temperature. *ISPRS J. Photogramm. Remote Sens.* **2017**, *124*, 119–132. [CrossRef]
91. Weng, Q.H.; Fu, P. Modeling annual parameters of clear-sky land surface temperature variations and evaluating the impact of cloud cover using time series of Landsat TIR data. *Remote Sens. Environ.* **2014**, *140*, 267–278. [CrossRef]
92. Mallick, J.; Rahman, A.; Singh, C.K. Modeling urban heat islands in heterogeneous land surface and its correlation with impervious surface area by using night-time ASTER satellite data in highly urbanizing city, Delhi-India. *Adv. Space Res.* **2013**, *52*, 639–655. [CrossRef]
93. Connors, J.P.; Galletti, C.S.; Chow, W.T.L. Landscape configuration and urban heat island effects: Assessing the relationship between landscape characteristics and land surface temperature in Phoenix, Arizona. *Landsc. Ecol.* **2013**, *28*, 271–283. [CrossRef]
94. Wentz, E.A.; Quattrochi, D.A.; Netzband, M.; Myint, S.W. Synthesizing urban remote sensing through application, scale, data and case studies. *Geocarto Int.* **2012**, *27*, 425–442. [CrossRef]
95. Xian, G.; Crane, M. An analysis of urban thermal characteristics and associated land cover in Tampa Bay and Las Vegas using Landsat satellite data. *Remote Sens. Environ.* **2006**, *104*, 147–156. [CrossRef]
96. Wilson, J.S.; Clay, M.; Martin, E.; Stuckey, D.; Vedder-Risch, K. Evaluating environmental influences of zoning in urban ecosystems with remote sensing. *Remote Sens. Environ.* **2003**, *86*, 303–321. [CrossRef]
97. Xian, G.Z.; Shi, H.; Auch, R.; Gallo, K.P.; Zhou, Q.; Wu, Z.; Kolian, M. The effects of urban land cover dynamics on urban heat island intensity and temporal trends. *GIScience Remote Sens.* **2021**. [CrossRef]
98. Howard, L. *The Climate of London, Deduced From Meteorological Observations, Made at Different Places in the Neighbourhood of the Metropolis*; Phillips, W., Ed.; George Yard: London, UK, 1818.
99. Stewart, I.D.; Oke, T.R.; Krayenhoff, E.S. Evaluation of the 'local climate zone' scheme using temperature observations and model simulations. *Int. J. Climatol.* **2014**, *34*, 1062–1080. [CrossRef]
100. US EPA. *Reducing Urban Heat Islands: Compendium of Strategies*; US EPA: Washington, DC, USA, 2008.
101. Martin-Vide, J.; Sarricolea, P.; Moreno-García, M.C. On the definition of urban heat island intensity: The "rural" reference. *Front. Earth Sci.* **2015**, *3*. [CrossRef]
102. Giridharan, R.; Emmanuel, R. The impact of urban compactness, comfort strategies and energy consumption on tropical urban heat island intensity: A review. *Sustain. Cities Soc.* **2018**, *40*, 677–687. [CrossRef]
103. Zhang, F.S.; Liu, Z.X. Fractal theory and its application in the analysis of soil spatial variability: A review. *J. Appl. Ecol.* **2011**, *22*, 1351–1358.
104. Gustafson, E.J. How has the state-of-the-art for quantification of landscape pattern advanced in the twenty-first century? *Landsc. Ecol.* **2019**, *34*, 2065–2072. [CrossRef]
105. Hu, L.Q.; Brunsell, N.A. A new perspective to assess the urban heat island through remotely sensed atmospheric profiles. *Remote Sens. Environ.* **2015**, *158*, 393–406. [CrossRef]
106. Hu, L.Q.; Monaghan, A.J.; Brunsell, N.A. Investigation of Urban Air Temperature and Humidity Patterns during Extreme Heat Conditions Using Satellite-Derived Data. *J. Appl. Meteorol. Climatol.* **2015**, *54*, 2245–2259. [CrossRef]

107. Tam, B.Y.; Gough, W.A.; Mohsin, T. The impact of urbanization and the urban heat island effect on day to day temperature variation. *Urban Clim.* **2015**, *12*, 1–10. [CrossRef]
108. Roth, M.; Oke, T.R.; Emery, W.J. Satellite-derived urban heat islands from three coastal cities and the utilization of such data in urban climatology. *Int. J. Remote Sens.* **1989**, *10*, 1699–1720. [CrossRef]
109. Lagouarde, J.P.; Moreau, P.; Irvine, M.; Bonnefond, J.M.; Voogt, J.A.; Solliec, F. Airborne experimental measurements of the angular variations in surface temperature over urban areas: Case study of Marseille (France). *Remote Sens. Environ.* **2004**, *93*, 443–462. [CrossRef]
110. Li, Y.; Schubert, S.; Kropp, J.P.; Rybski, D. On the influence of density and morphology on the Urban Heat Island intensity. *Nat. Commun.* **2020**, *11*, 2647. [CrossRef] [PubMed]
111. Ramírez-Aguilar, E.A.; Lucas Souza, L.C. Urban form and population density: Influences on Urban Heat Island intensities in Bogotá, Colombia. *Urban Clim.* **2019**, *29*. [CrossRef]
112. Paoletti, M.E.; Haut, J.M.; Plaza, J.; Plaza, A. Deep learning classifiers for hyperspectral imaging: A review. *ISPRS J. Photogramm. Remote Sens.* **2019**, *158*, 279–317. [CrossRef]
113. Zhang, L.; Zhang, L.; Du, B. Deep learning for remote sensing data: A technical tutorial on the state of the art. *IEEE Geosci. Remote Sens. Mag.* **2016**, *4*, 22–40. [CrossRef]
114. Chen, M.; Jiang, X.; Wu, H.; Wang, N.; Tang, R. An in-Scene Atmospheric Compensation Algorithm for Aster Thermal Band. In Proceedings of the International Geoscience and Remote Sensing Symposium (IGARSS), Yokohama, Japan, 28 July–2 August 2019; pp. 1876–1879. [CrossRef]
115. French, A.N.; Inamdar, A. Land cover characterization for hydrological modelling using thermal infrared emissivities. *Int. J. Remote Sens.* **2010**, *31*, 3867–3883. [CrossRef]
116. Sobrino, J.A.; Jiménez-Muñoz, J.C.; Sòria, G.; Romaguera, M.; Guanter, L.; Moreno, J.; Plaza, A.; Martínez, P. Land surface emissivity retrieval from different VNIR and TIR sensors. *IEEE Trans. Geosci. Remote Sens.* **2008**, *46*, 316–327. [CrossRef]
117. Mohamed, A.A.; Odindi, J.; Mutanga, O. Land surface temperature and emissivity estimation for Urban Heat Island assessment using medium- and low-resolution space-borne sensors: A review. *Geocarto Int.* **2017**, *32*, 455–470. [CrossRef]
118. Gillespie, A.; Rokugawa, S.; Matsunaga, T.; Steven Cothern, J.; Hook, S.; Kahle, A.B. A temperature and emissivity separation algorithm for advanced spaceborne thermal emission and reflection radiometer (ASTER) images. *IEEE Trans. Geosci. Remote Sens.* **1998**, *36*, 1113–1126. [CrossRef]
119. Rolim, S.B.A.; Grondona, A.; Hackmann, C.L.; Rocha, C. A Review of Temperature and Emissivity Retrieval Methods: Applications and Restrictions. *Am. J. Environ. Eng.* **2016**, *6*, 119–128. [CrossRef]
120. Li, Z.L.; Wu, H.; Wang, N.; Qiu, S.; Sobrino, J.A.; Wan, Z.; Tang, B.H.; Yan, G. Land surface emissivity retrieval from satellite data. *Int. J. Remote Sens.* **2013**, *34*, 3084–3127. [CrossRef]
121. Ma, M.; Chen, S.B.; Lu, T.Q.; Lu, P.; Xiao, Y. Study on scale problems based on the diviner thermal infrared emissivity of LRO satellite. *Hongwai Yu Haomibo Xuebao J. Infrared Millim. Waves* **2018**, *37*, 315–324. [CrossRef]
122. Wang, W.; Yao, X.; Shu, J. Air advection induced differences between canopy and surface heat islands. *Sci. Total Environ.* **2020**, *725*. [CrossRef]
123. Oláh, A.B. The possibilities of decreasing the urban heat Island. *Appl. Ecol. Environ. Res.* **2012**, *10*, 173–183. [CrossRef]
124. Gaur, A.; Eichenbaum, M.K.; Simonovic, S.P. Analysis and modelling of surface Urban Heat Island in 20 Canadian cities under climate and land-cover change. *J. Environ. Manag.* **2018**, *206*, 145–157. [CrossRef]
125. Cai, Z.; Han, G.; Chen, M. Do water bodies play an important role in the relationship between urban form and land surface temperature? *Sustain. Cities Soc.* **2018**, *39*, 487–498. [CrossRef]
126. Akbari, H.; Cartalis, C.; Kolokotsa, D.; Muscio, A.; Pisello, A.L.; Rossi, F.; Santamouris, M.; Synnefa, A.; Wong, N.H.; Zinzi, M. Local climate change and urban heat island mitigation techniques—The state of the art. *J. Civ. Eng. Manag.* **2016**, *22*, 1–16. [CrossRef]
127. Ulpiani, G.; Ranzi, G.; Shah, K.W.; Feng, J.; Santamouris, M. On the energy modulation of daytime radiative coolers: A review on infrared emissivity dynamic switch against overcooling. *Sol. Energy* **2020**, *209*, 278–301. [CrossRef]
128. Pickett, S.T.A.; Cadenasso, M.L.; Grove, J.M.; Boone, C.G.; Groffman, P.M.; Irwin, E.; Kaushal, S.S.; Marshall, V.; McGrath, B.P.; Nilon, C.H.; et al. Urban ecological systems: Scientific foundations and a decade of progress. *J. Environ. Manag.* **2011**, *92*, 331–362. [CrossRef] [PubMed]
129. Smargiassi, A.; Goldberg, M.S.; Plante, C.; Fournier, M.; Baudouin, Y.; Kosatsky, T. Variation of daily warm season mortality as a function of micro-urban heat islands. *J. Epidemiol. Community Health* **2009**, *63*, 659–664. [CrossRef] [PubMed]
130. Heaviside, C.; Vardoulakis, S.; Cai, X.M. Attribution of mortality to the urban heat island during heatwaves in the West Midlands, UK. *Environ. Health A Glob. Access Sci. Source* **2016**, *15*. [CrossRef] [PubMed]
131. Moon, J. The effect of the heatwave on the morbidity and mortality of diabetes patients; a meta-analysis for the era of the climate crisis. *Environ. Res.* **2021**, *195*. [CrossRef]
132. Li, J.; Xu, X.; Yang, J.; Liu, Z.; Xu, L.; Gao, J.; Liu, X.; Wu, H.; Wang, J.; Yu, J.; et al. Ambient high temperature and mortality in Jinan, China: A study of heat thresholds and vulnerable populations. *Environ. Res.* **2017**, *156*, 657–664. [CrossRef]
133. Tan, J.; Zheng, Y.; Tang, X.; Guo, C.; Li, L.; Song, G.; Zhen, X.; Yuan, D.; Kalkstein, A.J.; Li, F.; et al. The urban heat island and its impact on heat waves and human health in Shanghai. *Int. J. Biometeorol.* **2010**, *54*, 75–84. [CrossRef]

134. Johnson, D.P.; Wilson, J.S.; Luber, G.C. Socioeconomic indicators of heat-related health risk supplemented with remotely sensed data. *Int. J. Health Geogr.* **2009**, *8*, 57. [CrossRef] [PubMed]
135. Chen, L.; Jiang, R.; Xiang, W.N. Surface Heat Island in Shanghai and Its Relationship with Urban Development from 1989 to 2013. *Adv. Meteorol.* **2016**. [CrossRef]
136. Zhou, D.; Bonafoni, S.; Zhang, L.; Wang, R. Remote sensing of the urban heat island effect in a highly populated urban agglomeration area in East China. *Sci. Total Environ.* **2018**, *628–629*, 415–429. [CrossRef]
137. Zhou, B.; Rybski, D.; Kropp, J.P. The role of city size and urban form in the surface urban heat island. *Sci. Rep.* **2017**, *7*, 4791. [CrossRef]
138. Zhou, D.; Zhang, L.; Hao, L.; Sun, G.; Liu, Y.; Zhu, C. Spatiotemporal trends of urban heat island effect along the urban development intensity gradient in China. *Sci. Total Environ.* **2016**, *544*, 617–626. [CrossRef] [PubMed]
139. Adeyeri, O.E.; Akinsanola, A.A.; Ishola, K.A. Investigating surface urban heat island characteristics over Abuja, Nigeria: Relationship between land surface temperature and multiple vegetation indices. *Remote Sens. Appl. Soc. Environ.* **2017**, *7*, 57–68. [CrossRef]
140. Wu, X.; Cheng, Q. Coupling Relationship of Land Surface Temperature, Impervious Surface Area and Normalized Difference Vegetation Index for Urban Heat Island Using Remote Sensing. In Proceedings of the SPIE—The International Society for Optical Engineering 2007. Available online: https://www.spiedigitallibrary.org/conference-proceedings-of-spie/6749/1/Coupling-relationship-of-land-surface-temperature-impervious-surface-area-and/10.1117/12.737550.full?SSO=1 (accessed on 10 October 2020). [CrossRef]
141. Alexander, C. Normalised difference spectral indices and urban land cover as indicators of land surface temperature (LST). *Int. J. Appl. Earth Obs. Geoinf.* **2020**, *86*, 102013. [CrossRef]
142. Diaz-Pacheco, J.; Gutiérrez, J. Exploring the limitations of CORINE Land Cover for monitoring urban land-use dynamics in metropolitan areas. *J. Land Use Sci.* **2014**, *9*, 243–259. [CrossRef]
143. Giannakopoulos, C.; Kostopoulou, E.; Varotsos, K.V.; Tziotziou, K.; Plitharas, A. An integrated assessment of climate change impacts for Greece in the near future. *Reg. Environ. Chang.* **2011**, *11*, 829–843. [CrossRef]
144. Estrada, F.; Botzen, W.J.W.; Tol, R.S.J. A global economic assessment of city policies to reduce climate change impacts. *Nat. Clim. Chang.* **2017**, *7*, 403–406. [CrossRef]
145. Li, X.; Li, W.; Middel, A.; Harlan, S.L.; Brazel, A.J.; Turner, B.L. Remote sensing of the surface urban heat island and land architecture in Phoenix, Arizona: Combined effects of land composition and configuration and cadastral-demographic-economic factors. *Remote Sens. Environ.* **2016**, *174*, 233–243. [CrossRef]
146. Cai, G.Y.; Liu, Y.; Du, M.Y. Impact of the 2008 Olympic Games on urban thermal environment in Beijing, China from satellite images. *Sustain. Cities Soc.* **2017**, *32*, 212–225. [CrossRef]
147. Bonafoni, S.; Baldinelli, G.; Verducci, P. Sustainable strategies for smart cities: Analysis of the town development effect on surface urban heat island through remote sensing methodologies. *Sustain. Cities Soc.* **2017**, *29*, 211–218. [CrossRef]
148. Pickett, S.T.A.; Cadenasso, M.L.; Grove, J.M.; Nilon, C.H.; Pouyat, R.V.; Zipperer, W.C.; Costanza, R. Urban Ecological Systems: Linking Terrestrial Ecological, Physical, and Socioeconomic Components of Metropolitan Areas. *Annu. Rev. Ecol. Syst.* **2001**, *32*, 127–157. [CrossRef]
149. Ciardini, V.; Caporaso, L.; Sozzi, R.; Petenko, I.; Bolignano, A.; Morelli, M.; Melas, D.; Argentini, S. Interconnections of the urban heat island with the spatial and temporal micrometeorological variability in Rome. *Urban Clim.* **2019**, *29*. [CrossRef]
150. Čeplová, N.; Kalusová, V.; Lososová, Z. Effects of settlement size, urban heat island and habitat type on urban plant biodiversity. *Landsc. Urban Plan.* **2017**, *159*, 15–22. [CrossRef]
151. Coluzzi, R.; D'Emilio, M.; Imbrenda, V.; Giorgio, G.A.; Lanfredi, M.; Macchiato, M.; Ragosta, M.; Simoniello, T.; Telesca, V. Investigating climate variability and long-term vegetation activity across heterogeneous basilicata agroecosystems. *Geomat. Nat. Hazards Risk* **2019**, *10*, 168–180. [CrossRef]
152. Kaiser, A.; Merckx, T.; van Dyck, H. The Urban Heat Island and its spatial scale dependent impact on survival and development in butterflies of different thermal sensitivity. *Ecol. Evol.* **2016**, *6*, 4129–4140. [CrossRef]
153. Weng, Q.; Lu, D.; Schubring, J. Estimation of land surface temperature-vegetation abundance relationship for urban heat island studies. *Remote Sens. Environ.* **2004**, *89*, 467–483. [CrossRef]
154. Wang, H.T.; Zhang, Y.Z.; Tsou, J.Y.; Li, Y. Surface Urban Heat Island Analysis of Shanghai (China) Based on the Change of Land Use and Land Cover. *Sustainability* **2017**, *9*, 1538. [CrossRef]
155. Stathopoulou, M.; Cartalis, C.; Keramitsoglou, I. Mapping micro-urban heat islands using NOAA/AVHRR images and CORINE Land Cover: An application to coastal cities of Greece. *Int. J. Remote Sens.* **2004**, *25*, 2301–2316. [CrossRef]
156. Tran, H.; Uchihama, D.; Ochi, S.; Yasuoka, Y. Assessment with satellite data of the urban heat island effects in Asian mega cities. *Int. J. Appl. Earth Obs. Geoinf.* **2006**, *8*, 34–48. [CrossRef]
157. Zhang, Y.; Zhan, Y.; Yu, T.; Ren, X. Urban green effects on land surface temperature caused by surface characteristics: A case study of summer Beijing metropolitan region. *Infrared Phys. Technol.* **2017**, *86*, 35–43. [CrossRef]
158. Marina, S.; Constantinos, C. Study of the Urban Heat Island of Athens, Greece during Daytime and Night-Time. In Proceedings of the 2007 Urban Remote Sensing Joint Event, URS. Available online: https://www.researchgate.net/publication/4254319_Study_of_the_urban_heat_island_of_Athens_Greece_during_daytime_and_night-time (accessed on 5 May 2020). [CrossRef]

159. Liu, K.; Su, H.B.; Zhang, L.F.; Yang, H.; Zhang, R.H.; Li, X.K. Analysis of the Urban Heat Island Effect in Shijiazhuang, China Using Satellite and Airborne Data. *Remote Sens.* **2015**, *7*, 4804–4833. [CrossRef]
160. Ben-Dor, E.; Saaroni, H. Airborne video thermal radiometry as a tool for monitoring microscale structures of the urban heat island. *Int. J. Remote Sens.* **1997**, *18*, 3039–3053. [CrossRef]
161. Stathopoulou, M.; Cartalis, C. Downscaling AVHRR land surface temperatures for improved surface urban heat island intensity estimation. *Remote Sens. Environ.* **2009**, *113*, 2592–2605. [CrossRef]
162. Gallo, K.P.; Owen, T.W. Assessment of urban heat islands: A multi-sensor perspective for the Dallas-Ft. Worth, USA region. *Geocarto Int.* **1998**, *13*, 35–41. [CrossRef]
163. Zhi Qiao, Z.; Chen Wu, C.; Dongqi Zhao, D.; Xinliang Xu, X.; Jilin Yang, J.; Li Feng, L.; Sun, Z.; Liu, L. Determining the Boundary and Probability of Surface Urban Heat Island Footprint Based on a Logistic Model. *Remote Sens.* **2019**, *11*, 1368. [CrossRef]
164. Keramitsoglou, I.; Kiranoudis, C.T.; Ceriola, G.; Weng, Q.; Rajasekar, U. Identification and analysis of urban surface temperature patterns in Greater Athens, Greece, using MODIS imagery. *Remote Sens. Environ.* **2011**, *115*, 3080–3090. [CrossRef]
165. Ye, C.; Wang, M.J.; Li, J. Derivation of the characteristics of the surface urban heat island in the greater toronto area using thermal infrared remote sensing. *Remote Sens. Lett.* **2017**, *8*, 637–646. [CrossRef]
166. Kato, S.; Yamaguchi, Y. Estimation of storage heat flux in an urban area using ASTER data. *Remote Sens. Environ.* **2007**, *110*, 1–17. [CrossRef]
167. Lu, D.S.; Weng, Q.H. Spectral mixture analysis of ASTER images for examining the relationship between urban thermal features and biophysical descriptors in Indianapolis, Indiana, USA. *Remote Sens. Environ.* **2006**, *104*, 157–167. [CrossRef]
168. Sun, Y.; Gao, C.; Li, J.; Li, W.; Ma, R. Examining urban thermal environment dynamics and relations to biophysical composition and configuration and socio-economic factors: A case study of the Shanghai metropolitan region. *Sustain. Cities Soc.* **2018**, *40*, 284–295. [CrossRef]
169. Quan, J.L.; Zhan, W.F.; Chen, Y.H.; Wang, M.J.; Wang, J.F. Time series decomposition of remotely sensed land surface temperature and investigation of trends and seasonal variations in surface urban heat islands. *J. Geophys. Res. Atmos.* **2016**, *121*, 2638–2657. [CrossRef]
170. Gawuc, L.; Struzewska, J. Impact of MODIS Quality Control on Temporally Aggregated Urban Surface Temperature and Long-Term Surface Urban Heat Island Intensity. *Remote Sens.* **2016**, *8*, 374. [CrossRef]
171. Aniello, C.; Morgan, K.; Busbey, A.; Newland, L. Mapping micro-urban heat islands using LANDSAT TM and a GIS. *Comput. Geosci.* **1995**, *21*, 965–967, 969. [CrossRef]
172. Weng, Q.H. Fractal analysis of satellite-detected urban heat island effect. *Photogramm. Eng. Remote Sens.* **2003**, *69*, 555–566. [CrossRef]
173. Stathopoulou, M.; Cartalis, C. Daytime urban heat islands from Landsat ETM+ and Corine land cover data: An application to major cities in Greece. *Sol. Energy* **2007**, *81*, 358–368. [CrossRef]
174. Sagris, V.; Sepp, M. Landsat-8 TIRS Data for Assessing Urban Heat Island Effect and Its Impact on Human Health. *IEEE Geosci. Remote Sens. Lett.* **2017**, *14*, 2385–2389. [CrossRef]
175. Hulley, G.; Hook, S.; Fisher, J.; Lee, C. ECOSTRESS, A NASA Earth-Ventures Instrument for studying links between the water cycle and plant health over the diurnal cycle. In Proceedings of the International Geoscience and Remote Sensing Symposium (IGARSS), Fort Worth, TX, USA, 23–28 July 2017; pp. 5494–5496. [CrossRef]
176. Schultz, J.A.; Hartmann, M.; Heinemann, S.; Janke, J.; Jürgens, C.; Oertel, D.; Rücker, G.; Thonfeld, F.; Rienow, A. DIEGO: A Multispectral Thermal Mission for Earth Observation on the International Space Station. *Eur. J. Remote Sens.* **2019**. [CrossRef]
177. Elmes, A.; Rogan, J.; Williams, C.; Ratick, S.; Nowak, D.; Martin, D. Effects of urban tree canopy loss on land surface temperature magnitude and timing. *ISPRS J. Photogramm. Remote Sens.* **2017**, *128*, 338–353. [CrossRef]
178. Yan, L.; Roy, D.P. Spatially and temporally complete Landsat reflectance time series modelling: The fill-and-fit approach. *Remote Sens. Environ.* **2020**, *241*. [CrossRef]
179. Forster, B. Some urban measurements from Landsat data (Sydney, Australia). *Photogramm. Eng. Remote Sens.* **1983**, *49*, 1693–1707.
180. Zhao, W.; Li, A. A Review on Land Surface Processes Modelling over Complex Terrain. *Adv. Meteorol.* **2015**, *2015*. [CrossRef]
181. Nichol, J.E.; Fung, W.Y.; Lam, K.s.; Wong, M.S. Urban heat island diagnosis using ASTER satellite images and 'in situ' air temperature. *Atmos. Res.* **2009**, *94*, 276–284. [CrossRef]
182. Hirano, Y.; Yasuoka, Y.; Ichinose, T. Urban climate simulation by incorporating satellite-derived vegetation cover distribution into a mesoscale meteorological model. *Theor. Appl. Climatol.* **2004**, *79*, 175–184. [CrossRef]
183. Liou, Y.A.; Kar, S.K. Evapotranspiration estimation with remote sensing and various surface energy balance algorithms-a review. *Energies* **2014**, *7*, 2821–2849. [CrossRef]
184. Stone, B.; Norman, J.M. Land use planning and surface heat island formation: A parcel-based radiation flux approach. *Atmos. Environ.* **2006**, *40*, 3561–3573. [CrossRef]
185. Zubair, O.A.; Weilert, T. Potential Application of Change in Urban Green Space as an Indicator of Urban Environmental Quality Change. *Univers. J. Geosci.* **2014**, *2*, 222–228. [CrossRef]
186. Nichol, J.; Wong, M.S. Modeling urban environmental quality in a tropical city. *Landsc. Urban Plan.* **2005**, *73*, 49–58. [CrossRef]
187. Shin, M.; Kang, Y.; Park, S.; Im, J.; Yoo, C.; Quackenbush, L.J. Estimating ground-level particulate matter concentrations using satellite-based data: A review. *GISci. Remote Sens.* **2020**, *57*, 174–189. [CrossRef]

188. McDonald, R.I.; Kroeger, T.; Zhang, P.; Hamel, P. The Value of US Urban Tree Cover for Reducing Heat-Related Health Impacts and Electricity Consumption. *Ecosystems* **2019**. [CrossRef]
189. Arnfield, A.J. Two decades of urban climate research: A review of turbulence, exchanges of energy and water, and the urban heat island. *Int. J. Climatol.* **2003**, *23*, 1–26. [CrossRef]
190. Fu, P.; Xie, Y.; Weng, Q.; Myint, S.; Meacham-Hensold, K.; Bernacchi, C. A physical model-based method for retrieving urban land surface temperatures under cloudy conditions. *Remote Sens. Environ.* **2019**, *230*. [CrossRef]
191. Hulley, G.; Shivers, S.; Wetherley, E.; Cudd, R. New ECOSTRESS and MODIS land surface temperature data reveal fine-scale heat vulnerability in cities: A case study for Los Angeles County, California. *Remote Sens.* **2019**, *11*, 2136. [CrossRef]
192. Shen, H.F.; Huang, L.W.; Zhang, L.P.; Wu, P.H.; Zeng, C. Long-term and fine-scale satellite monitoring of the urban heat island effect by the fusion of multi-temporal and multi-sensor remote sensed data: A 26-year case study of the city of Wuhan in China. *Remote Sens. Environ.* **2016**, *172*, 109–125. [CrossRef]
193. Avdan, U.; Jovanovska, G. Algorithm for automated mapping of land surface temperature using LANDSAT 8 satellite data. *J. Sens.* **2016**, *2016*. [CrossRef]
194. Peng, J.; Qiao, R.; Liu, Y.; Blaschke, T.; Li, S.; Wu, J.; Xu, Z.; Liu, Q. A wavelet coherence approach to prioritizing influencing factors of land surface temperature and associated research scales. *Remote Sens. Environ.* **2020**, *246*. [CrossRef]
195. Tang, Y.Q.; Lan, C.Y.; Feng, H.H. Effect analysis of land-use pattern with landscape metrics on an urban heat island. *J. Appl. Remote Sens.* **2018**, *12*. [CrossRef]
196. Schwarz, N.; Schlink, U.; Franck, U.; Großmann, K. Relationship of land surface and air temperatures and its implications for quantifying urban heat island indicators—An application for the city of Leipzig (Germany). *Ecol. Indic.* **2012**, *18*, 693–704. [CrossRef]
197. Szymanowski, M.; Kryza, M. GIS-based techniques for urban heat island spatialization. *Clim. Res.* **2009**, *38*, 171–187. [CrossRef]
198. Firozjaei, M.K.; Weng, Q.; Zhao, C.; Kiavarz, M.; Lu, L.; Alavipanah, S.K. Surface anthropogenic heat islands in six megacities: An assessment based on a triple-source surface energy balance model. *Remote Sens. Environ.* **2020**, *242*. [CrossRef]
199. Schmitt, M.; Zhu, X.X. Data Fusion and Remote Sensing: An ever-growing relationship. *IEEE Geosci. Remote Sens. Mag.* **2016**, *4*, 6–23. [CrossRef]
200. Zhou, Q.; Xian, G.; Shi, H. Gap fill of land surface temperature and reflectance products in landsat analysis ready data. *Remote Sens.* **2020**, *12*, 1192. [CrossRef]
201. Huang, F.; Zhan, W.; Voogt, J.; Hu, L.; Wang, Z.; Quan, J.; Ju, W.; Guo, Z. Temporal upscaling of surface urban heat island by incorporating an annual temperature cycle model: A tale of two cities. *Remote Sens. Environ.* **2016**, *186*, 1–12. [CrossRef]
202. Peres, L.D.F.; Lucena, A.J.D.; Rotunno Filho, O.C.; França, J.R.D.A. The urban heat island in Rio de Janeiro, Brazil, in the last 30 years using remote sensing data. *Int. J. Appl. Earth Obs. Geoinf.* **2018**, *64*, 104–116. [CrossRef]
203. Fu, P.; Weng, Q. A time series analysis of urbanization induced land use and land cover change and its impact on land surface temperature with Landsat imagery. *Remote Sens. Environ.* **2016**, *175*, 205–214. [CrossRef]
204. Lee, S.J.; Balling, R.; Gober, P. Bayesian maximum entropy mapping and the soft data problem in urban climate research. *Ann. Assoc. Am. Geogr.* **2008**, *98*, 309–322. [CrossRef]
205. Yuan, F.; Bauer, M.E. Comparison of impervious surface area and normalized difference vegetation index as indicators of surface urban heat island effects in Landsat imagery. *Remote Sens. Environ.* **2007**, *106*, 375–386. [CrossRef]
206. Chen, F.; Yang, S.; Yin, K.; Chan, P. Challenges to quantitative applications of Landsat observations for the urban thermal environment. *J. Environ. Sci.* **2017**, *59*, 80–88. [CrossRef]
207. Pielke Sr, R.A.; Davey, C.A.; Niyogi, D.; Fall, S.; Steinweg-Woods, J.; Hubbard, K.; Lin, X.; Cai, M.; Kim, Y.K.; Li, H.; et al. Unresolved issues with the assessment of multidecadal global land surface temperature trends. *J. Geophys. Res. Atmos.* **2007**, *112*. [CrossRef]
208. Wong, K.V.; Chaudhry, S. Use of Satellite Images for Observational and Quantitative Analysis of Urban Heat Islands around the World. *J. Energy Resour. Technol. Trans. ASME* **2012**, *134*. [CrossRef]
209. Yan, Z.-W.; Wang, J.; Xia, J.-J.; Feng, J.-M. Review of recent studies of the climatic effects of urbanization in China. *Adv. Clim. Chang. Res.* **2016**, *7*, 154–168. [CrossRef]
210. Imhoff, M.L.; Zhang, P.; Wolfe, R.E.; Bounoua, L. Remote sensing of the urban heat island effect across biomes in the continental USA. *Remote Sens. Environ.* **2010**, *114*, 504–513. [CrossRef]
211. Coutts, A.M.; Harris, R.J.; Phan, T.; Livesley, S.J.; Williams, N.S.G.; Tapper, N.J. Thermal infrared remote sensing of urban heat: Hotspots, vegetation, and an assessment of techniques for use in urban planning. *Remote Sens. Environ.* **2016**, *186*, 637–651. [CrossRef]
212. Ruan, Y.L.; Zou, Y.H. Monitoring the Spatio-Temporal Trajectory of Urban Area Hotspots in Wuhan, China Using Time-Series Nighttime Light Images. *ISPRS Int. Arch. Photogramm. Remote Sens. Spat. Inf. Sci.* **2019**, 71–76. [CrossRef]
213. Chen, L.; Sun, R.; Lu, Y. A conceptual model for a process-oriented landscape pattern analysis. *Sci. China Earth Sci.* **2019**, *62*, 2050–2057. [CrossRef]
214. Jorgensen, S.E. *Integration of Ecosystem Theories: A Pattern*; 1992. Available online: https://link.springer.com/book/10.1007/978-94-011-2682-3 (accessed on 22 July 2021). [CrossRef]
215. Li, L.; Zha, Y. Satellite-based spatiotemporal trends of canopy urban heat islands and associated drivers in China's 32 major cities. *Remote Sens.* **2019**, *11*, 102. [CrossRef]

216. Li, J.X.; Song, C.H.; Cao, L.; Zhu, F.G.; Meng, X.L.; Wu, J.G. Impacts of landscape structure on surface urban heat islands: A case study of Shanghai, China. *Remote Sens. Environ.* **2011**, *115*, 3249–3263. [CrossRef]
217. Zhang, P.; Imhoff, M.L.; Wolfe, R.E.; Bounoua, L. Characterizing urban heat islands of global settlements using MODIS and nighttime lights products. *Can. J. Remote Sens.* **2010**, *36*, 185–196. [CrossRef]
218. Chen, W.; Zhang, Y.; Pengwang, C.Y.; Gao, W.J. Evaluation of Urbanization Dynamics and its Impacts on Surface Heat Islands: A Case Study of Beijing, China. *Remote Sens.* **2017**, *9*, 453. [CrossRef]
219. Schwarz, N.; Lautenbach, S.; Seppelt, R. Exploring indicators for quantifying surface urban heat islands of European cities with MODIS land surface temperatures. *Remote Sens. Environ.* **2011**, *115*, 3175–3186. [CrossRef]
220. Cheval, S.; Dumitrescu, A. The July urban heat island of Bucharest as derived from modis images. *Theor. Appl. Climatol.* **2009**, *96*, 145–153. [CrossRef]
221. Pan, J.H. Area Delineation and Spatial-Temporal Dynamics of Urban Heat Island in Lanzhou City, China Using Remote Sensing Imagery. *J. Indian Soc. Remote Sens.* **2016**, *44*, 111–127. [CrossRef]
222. Xu, Y.M.; Qin, Z.H.; Wan, H.X. Spatial and Temporal Dynamics of Urban Heat Island and Their Relationship with Land Cover Changes in Urbanization Process: A Case Study in Suzhou, China. *J. Indian Soc. Remote Sens.* **2010**, *38*, 654–663. [CrossRef]
223. Wang, J.; Kuffer, M.; Sliuzas, R.; Kohli, D. The exposure of slums to high temperature: Morphology-based local scale thermal patterns. *Sci. Total Environ.* **2019**, *650*, 1805–1817. [CrossRef]
224. De Noronha Vaz, E.; Cabral, P.; Caetano, M.; Nijkamp, P.; Painho, M. Urban heritage endangerment at the interface of future cities and past heritage: A spatial vulnerability assessment. *Habitat Int.* **2012**, *36*, 287–294. [CrossRef]
225. Larsen, L.G.; Eppinga, M.B.; Passalacqua, P.; Getz, W.M.; Rose, K.A.; Liang, M. Appropriate complexity landscape modeling. *Earth Sci. Rev.* **2016**, *160*, 111–130. [CrossRef]
226. Bala, R.; Prasad, R.; Yadav, V.P. Quantification of urban heat intensity with land use/land cover changes using Landsat satellite data over urban landscapes. *Theor. Appl. Climatol.* **2021**. [CrossRef]
227. Rajasekar, U.; Weng, Q.H. Urban heat island monitoring and analysis using a non-parametric model: A case study of Indianapolis. *ISPRS J. Photogramm. Remote Sens.* **2009**, *64*, 86–96. [CrossRef]
228. Szymanowski, M.; Kryza, M. Application of remotely sensed data for spatial approximation of urban heat island in the city of Wrocław, Poland. In Proceedings of the 2011 Joint Urban Remote Sensing Event, JURSE 2011—Proceedings, Munich, Germany, 11–13 April 2011; pp. 353–356. [CrossRef]
229. Audebert, N.; Le Saux, B.; Lefevre, S. Deep learning for classification of hyperspectral data: A comparative review. *IEEE Geosci. Remote Sens. Mag.* **2019**, *7*, 159–173. [CrossRef]
230. Bioucas-Dias, J.M.; Plaza, A.; Camps-Valls, G.; Scheunders, P.; Nasrabadi, N.M.; Chanussot, J. Hyperspectral remote sensing data analysis and future challenges. *IEEE Geosci. Remote Sens. Mag.* **2013**, *1*, 6–36. [CrossRef]
231. Sun, W.; Du, Q. Hyperspectral band selection: A review. *IEEE Geosci. Remote Sens. Mag.* **2019**, *7*, 118–139. [CrossRef]
232. Crisci, C.; Ghattas, B.; Perera, G. A review of supervised machine learning algorithms and their applications to ecological data. *Ecol. Model.* **2012**, *240*, 113–122. [CrossRef]
233. Lucas, T.C.D. A translucent box: Interpretable machine learning in ecology. *Ecol. Monogr.* **2020**, *90*. [CrossRef]
234. Gorelick, N.; Hancher, M.; Dixon, M.; Ilyushchenko, S.; Thau, D.; Moore, R. Google Earth Engine: Planetary-scale geospatial analysis for everyone. *Remote Sens. Environ.* **2017**, *202*, 18–27. [CrossRef]
235. Chu, L.; Oloo, F.; Bergstedt, H.; Blaschke, T. Assessing the link between human modification and changes in land surface temperature in hainan, china using image archives from google earth engine. *Remote Sens.* **2020**, *12*, 888. [CrossRef]
236. Hao, B.; Ma, M.; Li, S.; Li, Q.; Hao, D.; Huang, J.; Ge, Z.; Yang, H.; Han, X. Land use change and climate variation in the three gorges reservoir catchment from 2000 to 2015 based on the google earth engine. *Sensors* **2019**, *19*, 2118. [CrossRef]
237. Oleson, K.W.; Bonan, G.B.; Feddema, J.; Vertenstein, M. An urban parameterization for a global climate model. Part II: Sensitivity to input parameters and the simulated urban heat island in offline simulations. *J. Appl. Meteorol. Climatol.* **2008**, *47*, 1061–1076. [CrossRef]
238. Ghamisi, P.; Rasti, B.; Yokoya, N.; Wang, Q.; Hofle, B.; Bruzzone, L.; Bovolo, F.; Chi, M.; Anders, K.; Gloaguen, R.; et al. Multisource and multitemporal data fusion in remote sensing: A comprehensive review of the state of the art. *IEEE Geosci. Remote Sens. Mag.* **2019**, *7*, 6–39. [CrossRef]
239. Ghamisi, P.; Yokoya, N.; Li, J.; Liao, W.; Liu, S.; Plaza, J.; Rasti, B.; Plaza, A. Advances in Hyperspectral Image and Signal Processing: A Comprehensive Overview of the State of the Art. *IEEE Geosci. Remote Sens. Mag.* **2017**, *5*, 37–78. [CrossRef]
240. Sherafati, S.A.; Saradjian, M.R.; Niazmardi, S. Urban Heat Island growth modeling using Artificial Neural Networks and Support Vector Regression: A case study of Tehran, Iran. *Int. Arch. Photogramm. Remote Sens. Spatial Inf. Sci.* **2013**, 399–403. [CrossRef]
241. Brook, A.; de Micco, V.; Battipaglia, G.; Erbaggio, A.; Ludeno, G.; Catapano, I.; Bonfante, A. A smart multiple spatial and temporal resolution system to support precision agriculture from satellite images: Proof of concept on Aglianico vineyard. *Remote Sens. Environ.* **2020**, *240*. [CrossRef]
242. Ryo, M.; Angelov, B.; Mammola, S.; Kass, J.M.; Benito, B.M.; Hartig, F. Explainable artificial intelligence enhances the ecological interpretability of black-box species distribution models. *Ecography* **2021**, *44*, 199–205. [CrossRef]
243. Wulder, M.A.; Loveland, T.R.; Roy, D.P.; Crawford, C.J.; Masek, J.G.; Woodcock, C.E.; Allen, R.G.; Anderson, M.C.; Belward, A.S.; Cohen, W.B.; et al. Current status of Landsat program, science, and applications. *Remote Sens. Environ.* **2019**, *225*, 127–147. [CrossRef]

244. Shepherd, J.M.A.; Strother, C.T.; Horst, A.; Bounoua, L.; Mitra, C. *Urban Climate Archipelagos: A New Framework for Urban Impacts on Climate*; Earthzine: Washington, DC, USA, 2013. Available online: https://earthzine.org/urban-climate-archipelagos-a-new-framework-for-urban-impacts-on-climate/ (accessed on 13 August 2020).
245. Jeevalakshmi, D.; Narayana Reddy, S.; Manikiam, B. Land surface temperature retrieval from LANDSAT data using emissivity estimation. *Int. J. Appl. Eng. Res.* **2017**, *12*, 9679–9687.
246. Hayhoe, K.; VanDorn, J.; Croley, T.; Schlegal, N.; Wuebbles, D. Regional climate change projections for Chicago and the US Great Lakes. *J. Great Lakes Res.* **2010**, *36*, 7–21. [CrossRef]